Testing with $\delta^{44/40}$Ca and $\delta^{88/86}$Sr for ocean acidification during the Early Toarcian.

Q. Li [1,*], J..M. McArthur [1,2,#], M.F. Thirlwall [1], A.V. Turchyn [3], K. Page [4], H.J. Bradbury [3], R. Weis [5] and D. Lowry [1]

1. Earth Science, Royal Holloway University of London, Egham Hill, Egham, UK, TW20 0EX
2. Department of Earth Sciences, UCL, Gower Street, London WC1E 6BT, UK
3. Department of Earth Sciences, University of Cambridge, Cambridge, UK
4. University of Exeter, Penryn Campus, Penryn, Cornwall TR10 9FE,UK.
5. Palaeontological Department, National Museum of Natural History, 25 rue Münster, L-2160, Luxembourg, Grand-duchy of Luxembourg.

**Present address, Nu Instruments, Clywedog Road South, Wrexham, UK, LL13 9XS*
 # Corresponding author email: j.mcarthur@ucl.ac.uk

Abstract

During the Early Toarcian, volcanic gases released by the Karoo-Ferrar large igneous province are widely believed to have caused severe environmental disturbances, including ocean acidification and anoxia in marginal basins worldwide. Here we present records of $\delta^{44/40}$Ca and $\delta^{88/86}$Sr in biogenic calcite (belemnites and brachiopods) through the interval, which show no evidence of negative isotope excursions across the suggested acidification interval and so provides little support for ocean acidification at this time. The role of extreme volcanism in driving Early Toarcian environmental change therefore require re-examination.

Values of $\delta^{88/86}$Sr are independent of temperature or Sr/Ca. Values of $\delta^{44/40}$Ca correlate strongly and positively with temperature (0.020‰ /°C), suggesting that temperature is the dominant control on $\delta^{44/40}$Ca in the analysed belemnites and brachiopods. In belemnites, $\delta^{44/40}$Ca correlates positively with Mg/Ca and Sr/Ca.

Values of Mg/Ca correlate with temperatures measured by δ^{18}O and define the palaeo-temperature equation T°C = (2.02 ± 0.34)*Mg/Ca – (2.01 ± 2.8). The equation has large uncertainties that may be refined through suggested routes.

Keywords: Ca-isotopes, Sr-isotopes, Toarcian, OAE, ocean acidification.

1. Introduction

The Early Toarcian was a time of biotic change (Hallam 1986; Raup and Sepkoski 1986; Little and Benton 1995; Caswell *et al.* 2009; Danise *et al.* 2013). Although often referred to as a time of mass extinction (Little and Benton 1995), the biotic turnover was minor in comparison to the five most severe extinctions of the Phanerozoic and was an extended event (Little and Benton 1995; Harries and Little 1999). In addition to extinctions, originations, and environmental perturbations (*e.g.* Suan *et al.* 2008, 2010), organic-rich sediments were deposited in several locations around the world, *e.g.* Argentina (Al Suwaidi et al. 2009), Japan (Kemp and Izumi 2014), and China (Xu *et al.* 2017), whilst organic-poor sediments were deposited in some contemporaneous environments *e.g.* Peniche (Hesselbo *et al.* 2007) and Morocco (Bodin *et al.* 2010). Where it occurs, the organic-rich sedimentation is usually accompanied by a negative isotope shift in the $\delta^{13}C$ in organic matter. The shift is commonly reported to start in the uppermost *semicalatum I* Ammonite Subzone of the Tenuicostatum Ammonite Zone, reach a minimum in the mid-*exaratum* Subzone of the *Falciferum* Ammonite Zone and terminate at the end of that subzone (Küspert 1982; Hesselbo *et al.* 2000, 2007; *et seq;* Kemp *et al.* 2005).

The driver of both the shift in $\delta^{13}C_{org}$ and organic-rich sedimentation is often postulated to be volcanism of the Karoo-Ferrar large igneous province (Pálfy and Smith 2000; Burgess *et al.* 2015; Guex *et al.* 2016; Percival *et al.* 2016; many others). Radiometric dating place much of the eruptive phase of this volcanism in the latest Pliensbachian and earliest Toarcian (Jourdan *et al.* 2005, 2007, 2008; Burgess *et al.* 2015, Ivanov *et al.* 2017; Moulin *et al.* 2017). Copious amounts of carbon dioxide and sulphur dioxide may be emitted by LIP volcanism (Black *et al.* 2012; Schmidt *et al.* 2016). Dissolution of both gases in seawater (or lake water) might have caused ocean/lake acidification, leading to a suggestion that it did in *exaratum* times (Brazier *et al.* 2015; Müller *et al.* 2020).

Marine carbonates are isotopically lower than seawater in both $\delta^{44/40}Ca$ and $\delta^{88/86}Sr$ through preferential incorporation of ^{40}Ca over ^{44}Ca and ^{86}Sr over ^{88}Sr. At steady state, the isotopic compositions of Ca and Sr in seawater are therefore enriched in the heavier isotopes relative to carbonate sediments. Changing the rate or amount of carbonate sedimentation disturbs that equilibrium so the isotopic composition of Ca and Sr in the oceans may change correspondingly. Ocean acidification, by decreasing carbonate sedimentation and/or dissolving existing carbonate sediments, adds isotopically the lighter Ca and Sr isotopes to the ocean and generates negative excursions of both $\delta^{44/40}Ca$ and $\delta^{88/86}Sr$ in seawater, such as the excursions of ≈ -0.3 ‰ in $\delta^{44/40}Ca$ across the Permian-Triassic boundary (Payne *et al.* 2010) and ≈ -0.16‰ in $\delta^{44/40}Ca$ attributtable to ocean acidification across the Triassic-Jurassic boundary (Jost *et al.* 2017).

Here, we report $\delta^{44/40}$Ca and $\delta^{88/86}$Sr in macrofossil carbonate through a composite section spanning Early Toarcian time in order to look for isotopic indicators of ocean acidification in that interval. Our analysis also allows us to define a palaeo-temperature equation for belemnites relating Mg/Ca to temperature.

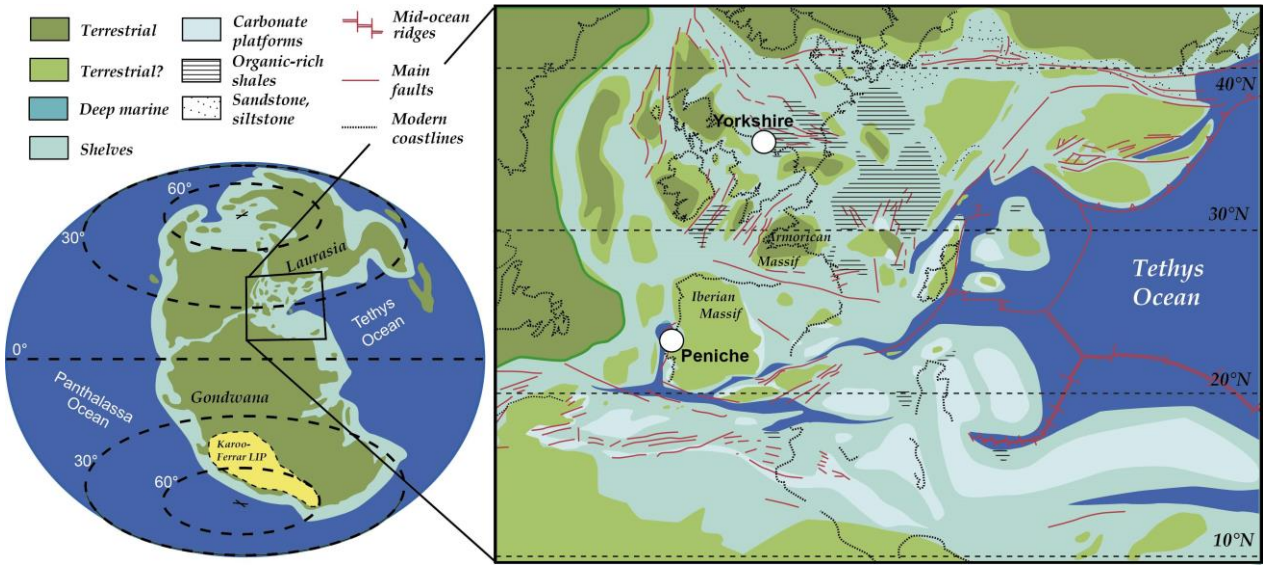

Fig. 1. Map showing the positions of the sections sampled in relation to the disposition of land masses across NW Europe during Early Toarcian time. Modified from Suan *et al.* (2018) after maps by Dera *et al.* (2009) and Thierry and Barrier (2000).

2. Study Areas and Samples

2.1. Stratigraphy

Our samples come from coastal exposures in Yorkshire, UK, and Peniche, Portugal (Fig. 1). The stratigraphy of both sections is summarized in Fig. 2, which also shows profiles of C-isotope variations through the interval derived from literature sources given in that figure's legend

The coastal sections at Peniche expose hemipelagic coccolith-bearing marls and limestones of the Lemede and Cabo Carvoeiro Formations, of Upper Pliensbachian and Lower Toarcian age. Ammonite biostratigraphy for Peniche has been provided by Mouterde (1955, 1967). Updates are provided by Elmi (2007); Rocha *et al.* (2016), Duarte *et al.* (2017) and Duarte *et al.* (2018). The lowermost Toarcian zone, the Tenuicostatum Zone, comprises a lower *mirabile* Subzone 20 cm thick overlain by an upper *semicelatum II* Subzone that is 11 m thick. The overlying Falciferum Zone at Peniche has no named subzones. The base of the Toarcian is at the base of the Bed 15e, the uppermost bed of the Lemede Formation. Peniche is the GSSP for the Toarcian Stage, despite contravening several of the requirements for such a choice, notably regarding the completeness and thickness of the section (Supplementary Information). Bed 15e encompasses the entire *mirabile*

Subzone and is highly condensed with severe condensation of Toarcian strata extending some 3 m above the boundary (McArthur *et al.* 2020a). A hiatus marks the base of the Falciferum Zone (Pittet *et al.* 2014).

The lithology and ammonite zonation of the Yorkshire sections are given in Howarth (1962; 1991) whose bed numbers are used here. The same ammonite zones are recognised in Peniche and Yorkshire (Page 2004; McArthur *et al.* 2020a). In Yorkshire, the Falciferum Zone is divided into a

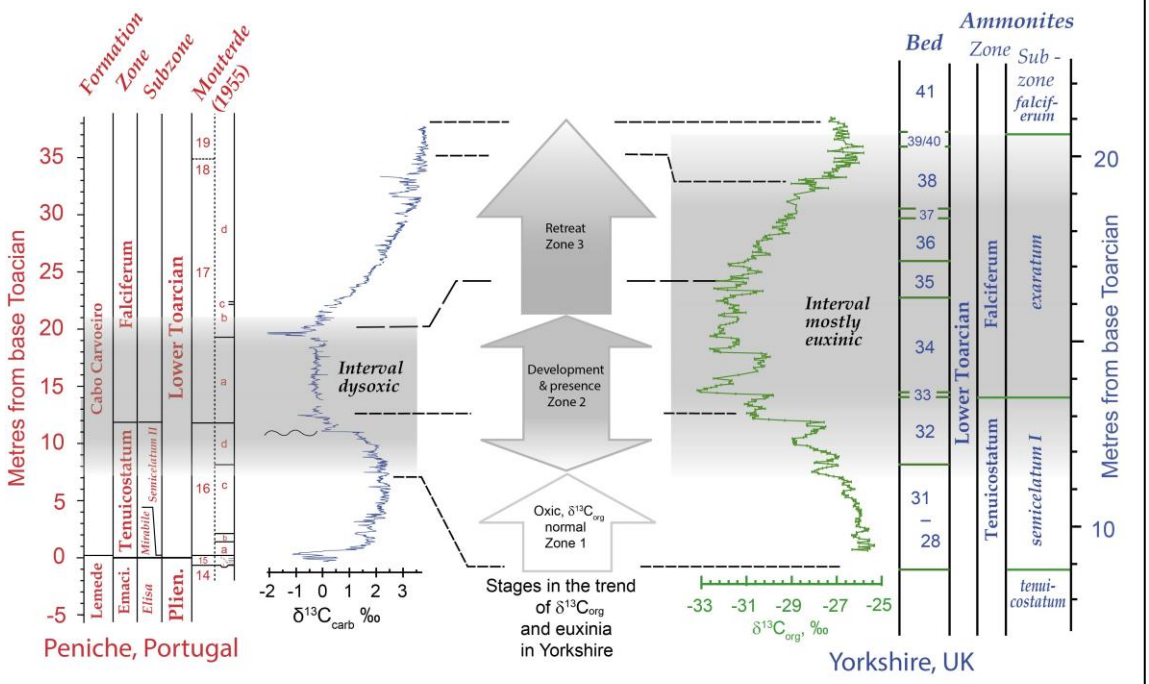

Fig. 2. Stratigraphy of the sections sampled in Peniche, Portugal, and Yorkshire, UK. Arrows denote the inception, development, and retreat of the driving force for the negative shift in $\delta^{13}C_{org}$ and euxinia in Yorkshire. Dysoxia in Peniche retreated before euxinia retreated from Yorkshire, whilst the C-isotope profiles are similar in both. The samples from Yorkshire are correlated to equivalent levels in Peniche using Sr-, C- and O-isotope stratigraphy (McArthur *et al.* 2000, 2020a). Values of $\delta^{13}C_{bulk\ carb}$ in Peniche from Hesselbo *et al.* (2007) and values of $\delta^{13}C_{org}$ in Yorkshire from Kemp *et al.* (2005).

lower *exaratum* Subzone and an overlying *falciferum* Subzone. The *exaratum* Subzone coincides with a lithological unit originally known as the Jet Rock, now renamed the lower part of the Mulgrave Shale Member of the Whitby Mudstone Formation. The interval from the uppermost *semicelatum I* Subzone to the top of the overlying *exaratum* Subzone (Bed 33 to top of Bed 40) are widely held to encompass the putative Toarcian oceanic anoxic event. The middle part of this interval is organic-rich with concentrations of total organic carbon (TOC) reaching 18%.

2.2. Environments

Peniche and Yorkshire show similar stratigraphic trends in trends in their carbon-isotope composition, with an interval of lower values between positive excursions in $\delta^{13}C$ at the top and bottom of the interval (Fig. 2). Numerous previous studies *e.g.* Röhl *et al.* (2001), Hesselbo *et al.*

(2000; 2007; others given below), have documented the fact that changes in $\delta^{13}C$ through the section occurred in parallel with changes in redox conditions of the water column in both localities, allowing three intervals of differing redox conditions in the water column to be identified (Fig. 2).

In Zone 1, conditions the water column at both localities appears to be oxic (benthic faunas are present) and values of $\delta^{13}C_{org}$ are around −25 ‰. Values of $\delta^{13}C_{carb}$ in the Tenuicostatum Zone at Peniche define the well-known positive excursion (Harazim *et al.* 2013; Bodin *et al.* 2016).

Zone 2 marks a decline in oxygenation of the water column that began in Yorkshire in the upper part of the *Semicelatum I* Subzone and developed into mostly euxinic conditions during *exaratum* times, the euxinia extending into the photic zone as shown by decreases in the size of framboidal pyrite in sediments (Wignall *et al.* 2005) and the presence in sediments of molecular biomarkers for photic-zone euxinia (Fig. 2; Schouten *et al.* 2000; French *et al.* 2014). Brief periods of oxygenation were recorded by short-lived invasions of benthos (*e.g.* Caswell *et al.* 2009, Caswell and Coe, 2013). In Peniche, development of such conditions was more subdued but occurred over the same interval. Upwards from the mid-Tenuicostatum Zone, the carbonate content of the sediment declines, nanno-plankton show increasing signs of stress (Suan *et al.* 2008) and belemnites become scarcer and smaller. The positive excursion in $\delta^{13}C_{bulk\ carb}$ that typifies much of Tenuicostatum time also diminishes. The bottom water in Peniche become dysoxic and unfavourable for benthos between 11 and 20 m in the section, during which time *in-situ* benthic macrofossils were absent and the sediments contain several percent dolomite (Hermoso 2009). The force driving the changes in both localities was initiated during late Tenuicostatum time.

In Zone 3, the force driving unfavourable conditions in the water column retreated and values of $\delta^{13}C$ increase in both localities to define the well-known positive isotope excursion that was for some time the recognised marker for the putative Early Toarcian oceanic anoxic event. Dysoxia had vanished from Peniche at the start of Zone 3 but euxinia persisted into the upper part of the *exaratum* Subzone in Yorkshire. Our brachiopod samples from Peniche were therefore alive during the euxinic interval in Yorkshire.

3. Sample preparation and analysis

3.1. Samples

Samples from Peniche were mostly belemnites of the family Passaloteuthididae, but the highest two stratigraphically, from Bed 133 at 35 m, are of the family Megateuthididae. The samples are a subset of those used to derive an $^{87}Sr/^{86}Sr$ profile through the section in Peniche (McArthur et al. 2020a). We also analysed four specimens of the brachiopod *Soaresirhynchia bouchardi*. No macrofossils were found between 11 m and 19 m in the section at Peniche. We filled this stratigraphic gap with six belemnites from the Whitby Mudstone Formation, Yorkshire, UK.

Of the Yorkshire samples, two (PM 13, PM 106) were used in McArthur *et al.* (2000a) and four were newly collected. Two belemnites derive from the uppermost part of Bed 32, in the uppermost *semicelatum I* Subzone, 20 – 40 cm below the base of the *exaratum* Subzone. Three belemnites are from the *exaratum* Subzone (Beds 34, 35, 38, of Howarth 1962). The sixth came from the *falciferum* Subzone of the *Falciferum* Zone at a level 10 cm above its base at the base of Bed 41. The lowest of the Yorkshire belemnites, from the upper part of Bed 32, belongs to the family Passaloteuthididae whilst the remainder are of the family Megateuthididae (Table 1).

3.2 Preparation

For belemnites, the exterior, the apical line, and other visually altered areas, were removed using diamond cutting tools. The samples were then broken into pieces and a piece of the stem region of the rostrum was crushed in an agate pestle-and-mortar. The fragments were immersed briefly (≈ 3 seconds) in 1.2 M hydrochloric acid to remove dust, rinsed with deionized water, and dried in a clean-hood. For analysis, fragments of mm or smaller size were picked from a methanol bath under the binocular microscope. Brachiopods were trimmed of adhering sediment using a scalpel and then gently crushed. Clean flakes of the inner shell were picked under the microscope for analysis. Analyzed fragments comprised translucent uncoloured calcite. Analyzed fragments were all exceptionally well preserved. Details of preservational state are given in the Supplementary Information, including photomicrographs of analyzed sampled (Fig. S1).

3.3. Measurements of $\delta^{44/40}$Ca

Measurements of $\delta^{44/40}Ca_{cal}$ were conducted on a Thermo Scientific Triton Plus Thermal ionization mass spectrometer (TIMS) at the University of Cambridge following the procedures in Bradbury and Turchyn (2018) and on a IsotopX Phoenix-X62 TIMS at Royal Holloway University of London (RHUL). At the University of Cambridge, samples were loaded onto double Re-filament assembly in nitrate format with H_3PO_4 as an activator, using a ^{42}Ca - ^{48}Ca double spike for mass fractionation correction. Replicate measurements of NIST SRM-915b standard yielded a mean $\delta^{44/40}$Ca of 0.76 ± 0.12 ‰ (2 s.d. n = 29) relative to SRM 915a. Samples measured at RHUL were loaded onto single Re filaments in nitrate with TaF_5 - H_3PO_4 emitter and using a pair of parafilm dams to minimize sample spread. A ^{43}Ca - ^{46}Ca double spike was used to corrected for mass fractionation. We report our values of $\delta^{44/40}Ca_{cal}$ relative SRM 915a. Replicates of an in-house Ca isotope standard HPS_{new} gave a mean $\delta^{44/40}$Ca value of 0.71 ± 0.20 ‰ (2 s.d. n = 11) relative to SRM 915a, a value consistent with its published values (Reynard *et al.* 2010; Li *et al.* 2016). ^{40}K interference on ^{40}Ca was monitored by measuring mass 41 and using the $^{40}K/^{41}K$ ratio of 0.0017384 for correction. The ^{40}K correction was only 1 – 2 ppm. The results of our analysis are given in Table 1.

Table 1. Elemental and isotopic compositions of belemnites and brachiopods analysed for this study. For $\delta^{44/40}Ca$ measurements, R = RHUL, C= Cambridge, For locality, Y = Yorkshire, P = Peniche, For taxonomy, M = Megateuthididae, H = Hastites, P = Passaloteuthididae, B = Brachiopod. Measured $\delta^{44/40}Ca_{calcite}$ to SRM 951a; measured $\delta^{88/86}Sr_{calcite}$ to SRM 987. Base values are measured values corrected for natural isotopic fractionation on precipitation of calcite from seawater.

										Measured		Base-	T-corr.	Detrend	Measured		Base-									
				Taxa	Site		Stratig.	Zone	Lab	$\delta^{44/40}Ca$	±	$\delta^{44/40}Ca$	$\delta^{44/40}Ca$	$\delta^{44/40}Ca$	$\delta^{88/86}Sr$	±	$\delta^{88/86}Sr$	$\delta^{13}C$	$\delta^{18}O$	Temp	Ca	Mg	Sr	Ba	Na	Fe	Mn
Stage	Ammonite	Ammonite	Sample No			Specimen identification:	Level,			Calcite	2 s.e.	Calcite	Calcite	Calcite	Calcite	2 s.e.	Calcite	Cal.	Cal.	Cal.	Cal.	Cal.	Cal.	Cal.	Cal.	Cal.	Cal.
	Zone	Subzone	and Bed No.			belemnites unless	m.a.d			to 915a		to 915a	to 915a	to 915a	SRM 987			‰V-PDB	‰V-PDB	°C	%	%	µg/g	µg/g	µg/g	µg/g	µg/g
						indicated otherwise	Peniche												-1								
Toarcian	Serpentinum	Exaratum Sz	PM 13	M	Y	?*Acrocoelites inaeqistriatus*	38.0	Zone 3	C	0.37	0.021	1.77	1.53	1.70	0.171	0.020	0.381	6.42	-3.30	26.4	38.9	0.305	1860	10	2678	31	4
Toarcian	Serpentinum	Exaratum Sz	PM 13 Repeat				38.0	Zone 3		0.29	0.022	1.69	1.46	1.63													
Toarcian	Serpentinum		133A	M	P	Acrocoelites sp	35.1	Zone 3	C	0.17	0.030	1.58	1.61	1.59	0.182	0.025	0.392	3.93	-0.44	13.3	39.4	0.267	1601	4	1976	56	5
Toarcian	Serpentinum		133A Repeat				35.1	Zone 3		0.16	0.022	1.56	1.60	1.58	0.184	0.034	0.394										
Toarcian	Serpentinum		133B	M	P	Indet.	35.1	Zone 3	C	0.20	0.019	1.60	1.60	1.60	0.182	0.018	0.392	3.51	-0.78	14.7	39.2	0.273	1275	5	1796	126	10
Toarcian	Serpentinum		133B Repeat				35.1	Zone 3		0.20	0.027	1.61	1.61	1.61													
Toarcian	Serpentinum	Exaratum Sz	Y18/PM/38(127/152)	M	Y	Acrocoelites sp	35.0	Zone 3	C	0.45	0.021	1.85	1.53	1.79	0.184	0.020	0.394	4.54	-4.22	31.0	39.2	0.307	1765	6	2542	46	7
Toarcian	Serpentinum	Exaratum Sz	Y18/PM/38(127/152) Repeat				35.0	Zone 3		0.25	0.021	1.65	1.33	1.59	0.191	0.036	0.401										
Toarcian	Serpentinum		13.3 m	B	P	*S. bouchardi* ?	25.8	Zone 3	C	0.64	0.022	1.49	1.37		0.187	0.040	0.397	3.40	-2.05	20.4	41.2	0.079	524	1	446	89	19
Toarcian	Serpentinum		12.4 m	B	P	*S. bouchardi* ?	24.9	Zone 3	C	0.87	0.018	1.72	1.61		0.167	0.029	0.377	3.47	-1.97	20.0	40.6	0.058	434	1	249	37	11
Toarcian	Serpentinum		12.0 m	B	P	*S. bouchardi* ?	24.5	Zone 3	C	0.80	0.021	1.65	1.52		0.168	0.031	0.378	3.21	-2.11	20.7	40.8	0.048	453	1	262	52	13
Toarcian	Serpentinum		9.65 m	B	P	*S. bouchardi* ?	22.2	Zone 3	C	0.76	0.021	1.61	1.46		0.223	0.030	0.433	1.87	-2.37	21.9	41.1	0.088	436	2	250	390	43
Toarcian	Serpentinum	Exaratum Sz	Y18/PM/35(0/91)	M	Y	Acrocoelites sp	20.0	Zone 2	C	0.38	0.020	1.78	1.47	1.71	1.390	0.028	1.600	0.84	-4.15	30.6	39.2	0.312	1585	6	2033	26	2
Toarcian	Serpentinum	Exaratum Sz	Y18/PM/34(173/259)	M	Y	Acrocoelites sp	16.0	Zone 2	C	0.53	0.020	1.93	1.57	1.72	0.219	0.022	0.429	1.22	-4.61	33.0	38.7	0.383	1700	17	2279	18	8
Toarcian	Serpentinum	Exaratum Sz	Y18/PM/34(173/259) Repeat				16.0	Zone 2		0.41	0.020	1.82	1.46	1.60													
Toarcian	Serpentinum	Semicelatum I	PM 106	M	Y	Acrocoelites sp	13.0	Zone 2	C	0.46	0.027	1.87	1.63	1.62	0.189	0.021	0.399	1.80	-3.30	26.4	38.3	0.395	1788	5	2130	7	8
Toarcian	Serpentinum	Semicelatum I	PM 106 Repeat				13.0	Zone 2		0.43	0.024	1.83	1.59	1.59	0.204	0.019	0.414				37.9	0.386	1787				
Toarcian	Serpentinum	Semicelatum I	PM 106 Repeat 2				13.0	Zone 2		0.46	0.028	1.86	1.62	1.62													
Toarcian	Serpentinum	Semicelatum I	Y18/KS/32(138/183)	P	Y	*cf. Pseudohastites longiformis* (juv.)	12.0	Zone 2	C	0.29	0.021	1.69	1.70	1.78	0.176	0.019	0.386	2.72	-0.74	14.6	39.1	0.227	1164	12	1415	60	18
Toarcian	Serpentinum	Semicelatum I	Y18/KS/32(138/183) Repeat				12.0	Zone 2		0.32	0.021	1.72	1.72	1.79	0.184	0.015	0.394	2.72	-0.89	15.2	39.7	0.241	1202				
Toarcian	Serpentinum	Semicelatum I	Y18/KS/32(138/183) Repeat 2				12.0	Zone 2		0.25	0.032	1.65	1.66	1.74				2.76	-0.74	14.6							
Toarcian	Tenuicostatum	Semicelatum II	25 B	P	P	Passaloteuthididae indet.	11.2	Zone 2	C	0.01	0.034	1.41	1.43	1.57	0.200	0.038	0.410	2.80	-0.69	14.4	40.1	0.197	1088	1	1240	11	2
Toarcian	Tenuicostatum	Semicelatum II	25 B Repeat				11.2	Zone 2		0.05	0.034	1.46	1.47	1.61							39.6	0.194	1076	2	673	32	5
Toarcian	Tenuicostatum	Semicelatum II	24 Top	P	P	Passaloteuthididae indet.	9.90	Zone 2	C	0.11	0.023	1.51	1.54	1.63	0.183	0.028	0.393	2.95	-0.47	13.4	39.4	0.209	1009	1	1145	18	2
Toarcian	Tenuicostatum	Semicelatum II	24 Top		P		9.90	Zone 2	R	0.01	0.051	1.41	1.44	1.53	0.212	0.028	0.422										
Toarcian	Tenuicostatum	Semicelatum II	22 Mid	P?	P	Indet	8.60	Zone 2	C	-0.08	0.054	1.32	1.34	1.49	0.164	0.025	0.374	3.49	-0.61	14.0	39.3	0.187	1126	1	1891	78	5
Toarcian	Tenuicostatum	Semicelatum II	22 Mid		P		8.60	Zone 2	R	0.05	0.091	1.45	1.47	1.61	0.228	0.035	0.438										
Toarcian	Tenuicostatum	Semicelatum II	21B	P	P	*Passaloteuthis* sp. indet.	7.40	Zone 1	C	0.06	0.031	1.46	1.45	1.66	0.194	0.025	0.404	3.35	-0.95	15.5	40.4	0.170	1193	1	1389	8	1
Toarcian	Tenuicostatum	Semicelatum II	21B		P		7.40	Zone 1	R	0.11	0.054	1.52	1.50	1.72													
Toarcian	Tenuicostatum	Semicelatum II	20	P	P	Passaloteuthididae indet.	7.10	Zone 1	C	0.05	0.031	1.45	1.47	1.63	0.207	0.025	0.417	2.43	-0.63	14.1	39.6	0.179	1018	1	673	23	2
Toarcian	Tenuicostatum	Semicelatum II	20		P		7.10	Zone 1	R	-0.01	0.057	1.39	1.41	1.57													
Toarcian	Tenuicostatum	Semicelatum II	17	P	P	Passaloteuthididae indet. juv.	5.00	Zone 1	C	0.08	0.022	1.48	1.49	1.62	0.159	0.029	0.369	2.78	-0.70	14.4	39.6	0.199	1047	1	1400	80	4
Toarcian	Tenuicostatum	Semicelatum II	15	P?	P	Indet	3.63	Zone 1	C	0.03	0.042	1.44	1.44	1.64	0.208	0.021	0.418	2.32	-0.81	14.9	40.0	0.171	1101	1	1371	50	5
Toarcian	Tenuicostatum	Semicelatum II	15		P		3.63	Zone 1	C	0.01	0.042	1.41	1.41	1.61													
Toarcian	Tenuicostatum	Semicelatum II	13 Top	P	P	*Passaloteuthis* sp. indet. juv.	3.10	Zone 1	C	-0.03	0.020	1.37	1.39	1.53	0.171	0.025	0.381	1.54	-0.64	14.1	40.0	0.193	1129	1	1313	22	2
Toarcian	Tenuicostatum	Semicelatum II	13 Top		P		3.10	Zone 1	R	0.09	0.058	1.50	1.51	1.65													
Toarcian	Tenuicostatum	Semicelatum II	11 Mid	P	P	Passaloteuthididae indet. juv.	1.70	Zone 1	C	0.20	0.024	1.60	1.60	1.79	0.156	0.029	0.366	1.88	-0.84	15.0	39.7	0.175	1076	1	1335	34	3
Toarcian	Tenuicostatum	Semicelatum II	11 Mid Repeat				1.70	Zone 1		0.09	0.020	1.49	1.49	1.68													
Toarcian	Tenuicostatum	Semicelatum II	7 Top	P	P	Passaloteuthididae indet.	1.20	Zone 1	C	-0.02	0.020	1.39	1.42	1.63	0.194	0.021	0.404	1.05	-0.44	13.3	40.2	0.147	1098	1	1100	2	1
Toarcian	Tenuicostatum	Semicelatum II	3C	P	P	Passaloteuthididae indet.	0.72	Zone 1	C	0.00	0.025	1.41	1.41	1.61	0.160	0.025	0.370	0.62	-0.79	14.8	39.8	0.169	1096	5	917	20	2
Toarcian	Tenuicostatum	Semicelatum II	3C Repeat				0.72	Zone 1		0.12	0.038	1.52	1.52	1.72							39.7	0.169	1092	1	588	29	2
Toarcian	Tenuicostatum	Semicelatum II	3C		P		0.72	Zone 1	R	0.07	0.059	1.47	1.48	1.68													
Toarcian	Tenuicostatum	Semicelatum II	2	P?	P	?*Pseudohastites* sp. A	0.39	Zone 1	C	0.18	0.025	1.58	1.61	1.74	0.178	0.025	0.388	0.54	-0.53	13.7	39.9	0.194	1205	1	1331	10	2
Toarcian	Tenuicostatum	Semicelatum II	2		P		0.39	Zone 1	R	0.09	0.060	1.49	1.52	1.65													
		Means, 2s.e.	**Zone 3 excluding brachs**										**1.535**	**1.636**	**0.182**	**0.003**	**0.392**										
		Means, 2s.e.	**Zone 3 incl brachs**										**1.521**		**0.184**	**0.005**	**0.394**										
		Means, 2s.e.	**Zone 2**										**1.540**	**1.640**	**0.304**	**0.114**	**0.514**										
		Means, 2s.e.	**Zone 1**										**1.477**	**1.654**	**0.181**	**0.007**	**0.391**										

3.4. Fractionation corrections: $\delta^{44/40}Ca$

We seek to define the variations through time in the $\delta^{44/40}Ca$ of seawater, so factors affecting the fractionation of Ca-isotopes into marine biogenic calcite must be corrected for. These factors are mineralogy (aragonite *v* calcite), taxonomic group/vital effects (fractionation factors for belemnites differ from those for brachiopods, Gussone *et al.* 2005; Farkaš *et al.* 2007a), temperature (*e.g.* Nägler et al. 2000; von Allmen *et al.* 2010; Gussone & Heuser 2016), and kinetics/rate of calcification (Kisakürek *et al.* 2011). The original mineralogy of the brachiopods, and the belemnite rostra, we have analysed was calcite, so there is no mineralogical control on our data. We correct for other controls as follows.

Taxonomic group: to account for the fact that we have analysed belemnites and brachiopods, we convert from measured $\delta^{44/40}Ca_{cal}$ to what we term here base-$\delta^{44/40}Ca_{cal}$ using fractionations of 1.4 ‰ for belemnites (Farkaš *et al.* 2007a) and 0.85 ‰ for brachiopods (Gussone *et al.* 2005). This correction converts $\delta^{44/40}Ca_{cal}$ to the $\delta^{44/40}Ca$ of the fluid from which they precipitate, which should be the $\delta^{44/40}Ca$ of seawater.

Temperature: base-$\delta^{44/40}Ca_{cal}$ were corrected to a common temperature of 15° C using a temperature dependence of Ca-isotope fractionation of +0.020 ‰/°C derived from the slope of the regression line in Fig. 3a between base-$\delta^{44/40}Ca_{cal}$ and temperature. We use the term temperature-corrected-$\delta^{44/40}Ca_{cal}$ for the result. Both brachiopods and belemnites fall on the regression line in Fig. 3a. The temperature dependency of +0.020 ‰/°C is similar in magnitude and sign to that reported by others (*e.g.* Gussone and Heuser 2016; but see also Farkaš *et al.* 2007a,b).

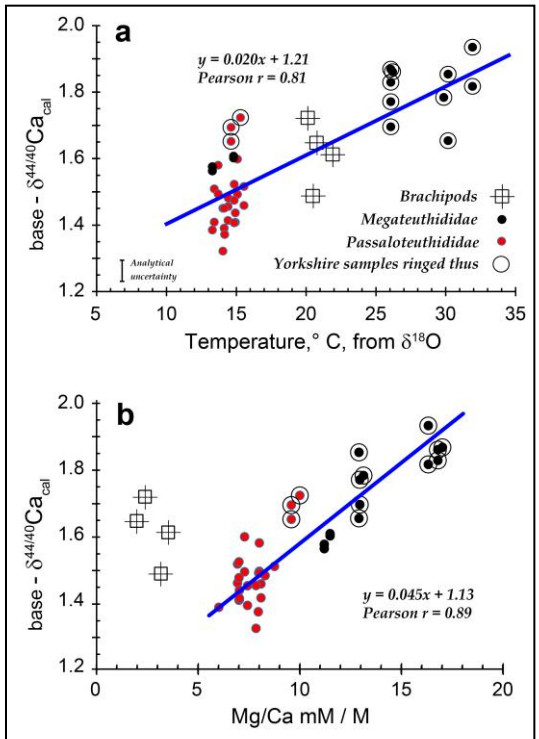

Fig. 3. Correlations of base-$\delta^{44/40}Ca_{cal}$ to **a**) temperature for all samples and **b**) Mg/Ca for belemnites. Temperatures are derived from $\delta^{18}O$ (Table 1) using the palaeo-temperature equation of Hays and Grossman (1991), and a value of −1 ‰ for $\delta^{18}O_{sw}$ for a world lacking ice-caps.

The positive correlation between base-$\delta^{44/40}Ca_{cal}$ and temperature (Fig. 3a) might be interpreted as suggesting that isotope fractionation of oxygen into belemnites is controlled by kinetic isotope fractionation, not equilibrium isotope fractionation (McConnaughey 1989; Watkins *et al.* 2013; Daëron *et al.* 2019). Values of $\delta^{18}O$ do not correlate with $\delta^{13}C$ (Fig. S2, Supplementary Information) as would be expected were kinetic isotope-effects influencing oxygen isotope compositions (see also Uchikawa and Zeebe 2012), so we discount kinetic isotope fractionation as significant either in generating the correlation seen in

Fig. 3a, or as a contributor to the scatter in Fig. 3a.

Calcification rate: in the analysed belemnites, $\delta^{44/40}Ca_{cal}$ correlates positively with Mg/Ca and Sr/Ca (Fig. 3b and Fig. 4a). A strong inverse relation between $\delta^{44/40}Ca_{cal}$ and Sr/Ca in inorganic calcite was found experimentally by Tang (2008) and ascribed to kinetic isotope fractionation governed by precipitation (calcification) rate. Modelling and measurement has subsequently confirmed these findings (DePaolo 2011; Nielsen *et al.* 2012). The absence in our samples of an inverse correlation between $\delta^{44/40}Ca_{cal}$ and Sr/Ca shows either that the results of inorganic experiments must be applied with caution to biogenic calcite or that calcification rate has only little or no influence on $\delta^{44/40}Ca$ in our samples. The latter deduction agrees with the observation of Ullmann and Pogge von Strandmann (2017) that, for a single specimen of *Passaloteuthis bisulcata* (Blainville, 1827), calcification-rate affected Mg/Ca minimally, with Mg/Ca *decreasing* by around 8% for a doubling of growth rate.

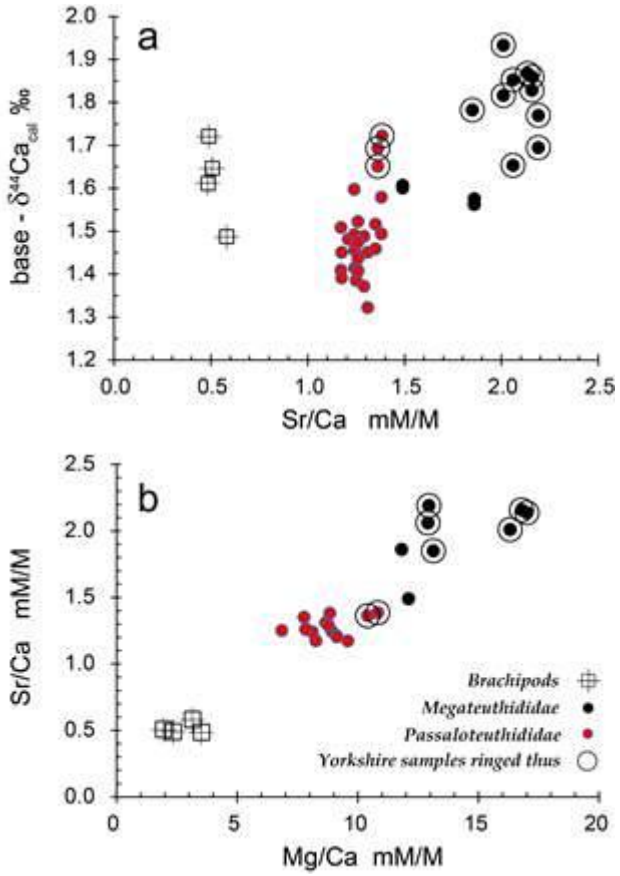

Fig. 4. Relation between Sr/Ca, base-$\delta^{44/40}Ca_{cal}$ and Mg/Ca. Symbols as on previous diagrams.

For belemnites, values of Mg/Ca correlate with base-$\delta^{44/40}Ca_{cal}$ (Fig. 3b, r = 0.89) more strongly than do temperatures (r = 0.82) and more strongly than the two variables correlate for the entire data set (Fig. 3a, r = 0.81). The improved correlation implies that base-$\delta^{44/40}Ca_{cal}$ in the belemnites might be marginally influenced by variations in precipitation rate and that correcting to a common Mg/Ca, rather than a common temperature, might correct for these marginal effects (*c.f.* Ullmann and Pogge von Strandmann 2017). We correct base-$\delta^{44/40}Ca_{cal}$ to a common Mg/Ca of 11.5 mM/M using the slope of the correlation line in Fig. 3b ($\Delta\delta^{44/40}Ca/\Delta Mg/Ca$ of 0.045). The term detrended-$\delta^{44/40}Ca_{cal}$ is applied to the result. The value of 11.5 does not represent the Mg/Ca of Early Toarcian seawater; the number is a convention adopted to bring all data to a common baseline. We use 11.5 because it is the middle value of the range of Mg/Ca of the samples; its use therefore minimizes changes to $\delta^{44/40}Ca_{cal}$. Other values could be used but with essentially similar results – to reduce value of Mg/Ca to a common baseline. The correction does not apply to the brachiopods, so brachiopods are omitted from consideration when detrended-$\delta^{44/40}Ca_{cal}$ is discussed in later sections.

3.5. Measurement of $\delta^{88/86}Sr$

Strontium isotope analyses were performed on the IsotopX Phoenix-X62 TIMS at Royal Holloway University of London (RHUL). The machine was run in multi-dynamic mode with correction for ^{87}Rb. Samples were dissolved in sub-boiled 8 M HNO_3, purified using Sr-Spec resin, and loaded as nitrate on a single Re filament with TaF_5 - H_3PO_4 emitter. An ^{87}Sr - ^{84}Sr double spike solution was used to correct for mass fractionation. Spiked and unspiked samples were prepared and run separately for $\delta^{88/86}Sr$ and $^{87}Sr/^{86}Sr$ analysis. During the course of the analysis, SRM 987 and IAPSO seawater were analysed as primary and secondary standards to monitor the performance of Sr measurements and to check the accuracy of the double spike correction method. The 31 measurements of SRM 987 yield an average $^{84}Sr/^{86}Sr$ of 0.056487 ± 0.000009, and a mean $^{87}Sr/^{86}Sr$ of 0.710239 ± 0.000009. The mean $\delta^{88/86}Sr$ of IAPSO seawater measured during this study was 0.390 ± 0.009 ‰ (2.s.e., *n* = 20), consistent with the published value of 0.386 ± 0.010 (2.s.e., *n* = 10; Krabbenhöft *et al.* 2009). The estimated analytical uncertainty of the measurements at 2 × s.d. is ± 0.04 ‰. The results of our analysis are tabulated as measured values in Table 1.

3.6. Fractionation Corrections: $\delta^{88/86}Sr$

We seek to define the variations through time in the $\delta^{88/86}Sr$ of seawater, so factors affecting the fractionation of Sr isotopes into marine biogenic calcite must be corrected for. These factors are temperature, taxonomic group, rate of precipitation and (possibly) mineralogy *i.e.* aragonite *v* calcite (Fietzke and Eisenhauer 2006; Böhm *et al.* 2012; Vollstaedt *et al.* 2014; Al-Khatib and Eisenhauer 2017). As we analysed only calcite, a mineralogical control is absent.

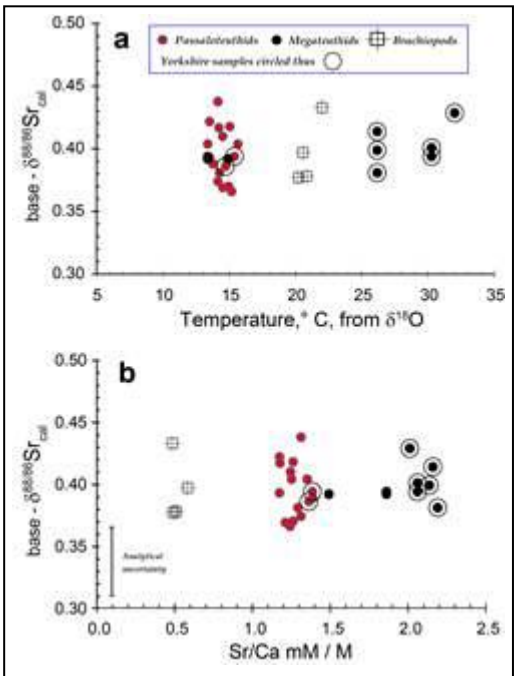

Fig. 5. Base-$\delta^{88/86}Sr_{cal}$ does not correlate with either **a**) temperature or **b**) Sr/Ca.

Taxonomic group: we can identify no taxonomic effect that preferentially biases isotopic composition any of the three groups analysed – Megateuthididae, Passaloteuthididae, or brachiopods, despite differences in Mg/Ca and Sr/Ca between these groups. Follow Vollstaedt *et al.* (2014), we therefore convert from measured $\delta^{88/86}Sr_{cal}$ to the values of $\delta^{88/86}Sr_{cal}$ that samples would have had were fractionation zero, and do so using a blanket fractionation factor of 0.21 ‰; that is, we add 0.21 ‰ to measured values of $\delta^{88/86}Sr_{cal}$. The result is termed base-$\delta^{88/86}Sr_{cal}$.

Temperature: in our samples, temperature does not correlate with base-$\delta^{88/86}Sr_{cal,}$ either overall or in any taxonomic group (Fig. 4a), so we do not correct for temperature dependency. Little temperature dependence has been reported for the calcitic foraminifera *G. ruber* (Böhm *et al.* 2012) and for modern calcitic terebratulid brachiopods (Vollstaedt *et al.* 2014). For the modern aragonitic coral *Pavona clavus*, Fietzke and Eisenhauer (2006) reported a dependence of +0.033 ‰ / °C.

Calcification rate: an inverse correlation between $\delta^{88/86}Sr_{cal}$ and Sr/Ca for biogenic calcite has been reported (Böhm *et al.* 2012) and appears also to extend to inorganic calcite (Al-Khatib and Eisenhauer 2017). The latter show that a single inverse correlation fits both inorganic calcite and biogenic calcite from a range of taxa. The inverse relation is ascribed to a kinetic control on the incorporation of Sr into the biogenic calcite structure (Stoll and Schrag, 2000 *et seq.*). In our samples $\delta^{88/86}Sr_{cal}$ is independent of Sr/Ca (Fig. 5b), so we make no correction for calcification rate.

3.7. Measurement of $\delta^{13}C$ and $\delta^{18}O$ and elemental composition

Analysis of calcite for $\delta^{13}C$ and $\delta^{18}O$ was done at RHUL using a GV Instruments (now Elementar) Multiflow prep system on line to an IsoPrime mass spectrometer. Standards used were NBS 19 and LSVEC international standards and RHUL internal calcite standard. External precision (2s.d.) of standards during the period of sample analysis was $\leq \pm 0.10$ ‰ for $\delta^{13}C$ and $\leq \pm 0.20$ ‰ for $\delta^{18}O$. At UCL, analysis of calcite for $\delta^{13}C$ and $\delta^{18}O$ was done using a Thermo Delta Plus XP mass spectrometer attached to a Thermo Gas Bench II device and a CTC Pal auto-sampler. Calibration was with in-house standard and NBS 19. External precision (2s.d.) of standards during the period of sample analysis was ≤ 0.04 ‰ for $\delta^{13}C$ and ≤ 0.1 ‰ for $\delta^{18}O$.

To measure elemental composition, samples of 10 mg were dissolved overnight in 10 ml of 2% nitric acid and, after appropriate dilution, were analysed for Ca, Ba, Fe, and Mn by direct comparison of intensities to the intensities of synthetic standards using a Varian 720 ICP-AES. Values of Mg/Ca and Sr/Ca were obtained by the intensity-ratio method of de Villiers (2002) and used to calculate Sr and Mg values from measured Ca.

4. Results and Discussion

4.1. Stratigraphic profile of $\delta^{44/40}Ca$

For presentation of the stratigraphic profile of $\delta^{44/40}Ca_{cal}$ (Fig. 6) we show base values in (a); temperature-corrected values in (b), and detrended-values in (c). The mean and 2 × s.e. for $\delta^{44/40}Ca_{cal}$ in Zones 1, 2 and 3 respectively given in Table 1. Values of base-$\delta^{44/40}Ca_{cal}$ (Fig. 6a) decrease by around 0.05‰ through the Tenuicostatum Zone then, up-section, show a positive

excursion of around 0.4 ‰ through the early part of the euxinic interval followed by decreasing values to the top of the section.

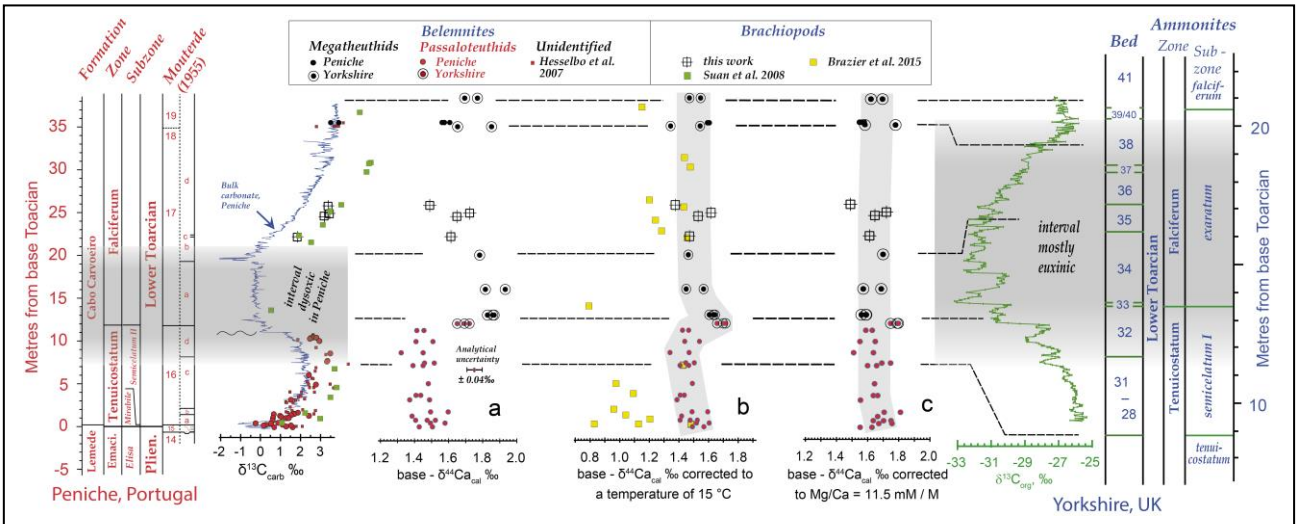

Fig. 6. Profiles of $\delta^{44/40}Ca_{cal}$ through the studied sections: **a)** base-$^{44/40}Ca_{cal}$ **b)** base-$\delta^{44/40}Ca_{cal}$ corrected to 15°C, with temperature calculated from $\delta^{18}O_{cal}$, a seawater of $\delta^{18}O$ = −1 ‰, and the temperature dependency on fractionation of 0.020 ‰/°C (Fig. 3a). Also shown are the data of Brazier *et al.* (2015) corrected to 15°C; **c)** detrended-$\delta^{44/40}Ca_{cal}$ (corrected Mg/Ca = 11.5 mM/M). Values of $\delta^{13}C_{cal}$ from this work, with additional data for Peniche from Hesselbo *et al.* (2007). Values of $\delta^{13}C_{org}$ in Yorkshire from Kemp *et al.* (2005).

Temperature-corrected values (Fig. 6b) are around 1.50 ‰ at the base of the section, decrease to 1.45 ‰ at around 8 m before showing a small positive spike of around 0.25 ‰ at the beginning of the *exaratum* Subzone. Values then decrease up-section to around 1.45 ‰ at the top of the profile. The most positive 30% of the temperature-corrected $\delta^{44/40}Ca_{cal}$ of Brazier *et al.* (2015; also corrected to 15°C) agrees well with our temperature-corrected $\delta^{44/40}Ca_{cal}$. Values of detrended-$\delta^{44/40}Ca_{cal}$ (Fig. 6c) show a small decline of around 0.05 ‰ from the base of the section to around the 3 m level, above which the trend appears unchanged to the top of the section apart from a possible positive blip of 0.1 ‰ at the top of the semicelatum 1 subzone which is smoothed away on Fig 6. The key point made in Fig. 6 is that, no matter what correction is applied, no profile shows a negative excursion of $\delta^{44/40}Ca_{cal}$ in the interval between the mid *semicelatum I* and lower *exaratum* subzones (Zone 2, Fig. 2).

4.2. Stratigraphic profile of $\delta^{88/86}Sr$

In Fig. 7 we show the profile of $\delta^{88/86}Sr$ against stratigraphic level. Values increase from around 0.39 ‰ at the base of the section to 0.41 ‰ at 8 – 20 m, and then decrease towards 0.39 ‰. At the top of the section. These changes are half our standard reproducibility of ± 0.040% (2.s.d). The data for the Yorkshire belemnites are indistinguishable from the trend defined by belemnites

and brachiopods from Peniche. The key point of Fig. 7 is that the profile does not show a negative excursion of $\delta^{88/86}Sr_{cal}$ in Zone 2 (Fig. 2, mid *semicelatum* to early *exaratum* time), the time when the driving force for the negative shift in $\delta^{13}C_{org}$, and so the putative ocean acidification, must have operated. The means and 2 × s.e. of base-$\delta^{88/86}Sr_{cal}$ in Zones 1, 2, and 3, respectively are given in Table 1.

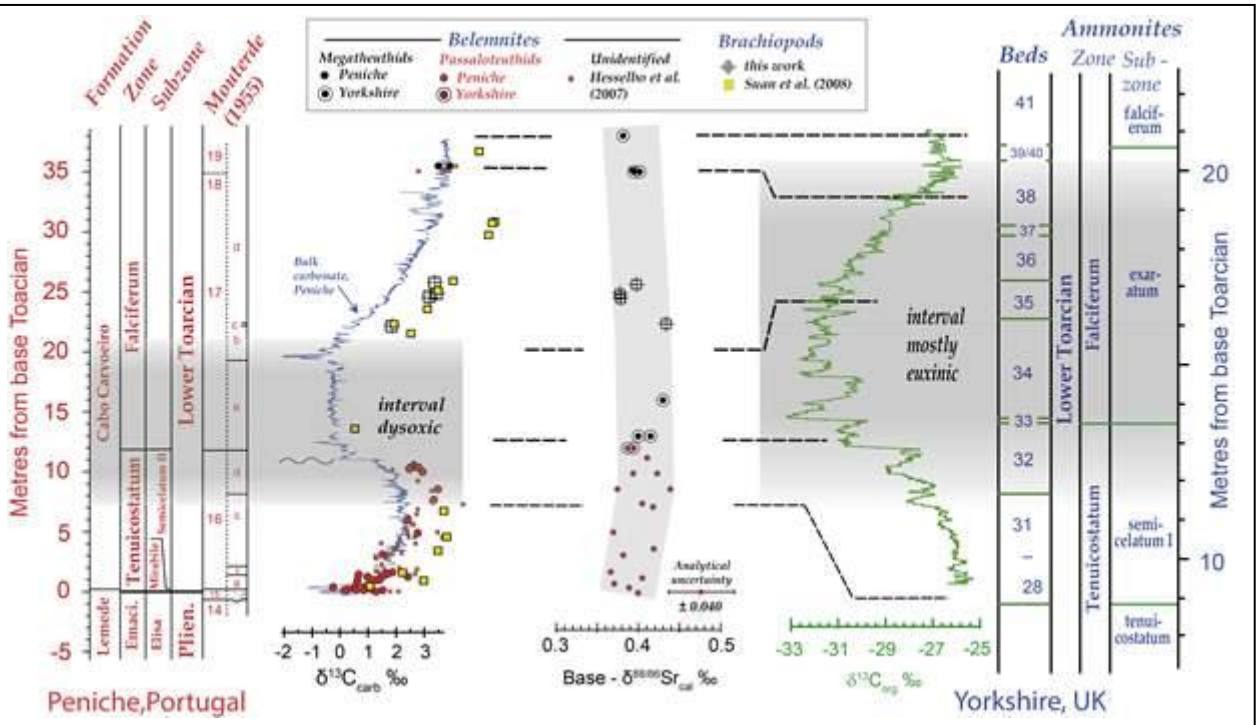

Fig. 7. Profile of base-$\delta^{88/86}Sr_{cal}$ through the sections at Peniche, Portugal, and Yorkshire, UK. The samples from Yorkshire are correlated to equivalent levels in Peniche using Sr-, C- and O-isotope stratigraphy (McArthur *et al.* 2000, 2020a). Other data sources as in Fig. 6.

4.3. $\delta^{44/40}$Ca: a model for comparison

To test for the causes of isotopic excursions, or their absence, in Ca and C through the study interval, we compare our stratigraphic profiles of $\delta^{44/40}Ca_{cal}$ and $\delta^{13}C_{org}$ to the models of Silva-Tamayo *et al.* (2018) These authors used a coupled biogeochemical calcium and carbon model to simulate the effect on $\delta^{13}C$ and $\delta^{44/40}Ca$ in seawater for four scenarios; the three relevant to this study are shown schematically in Fig. 8: *viz.* A, ocean acidification as a result of increased atmospheric CO_2 from LIP volcanism; B, increase in alkalinity (leading to an increase in precipitation rate of calcite/aragonite); C, increase in weathering and so increased nutrient flux to the ocean, leading to increased flux of organic matter to the ocean floor and so increased burial of ^{12}C-enriched carbon. Each model predicts the sense of isotopic excursions in $\delta^{44/40}Ca$ and $\delta^{13}C$ that would occur if driven by each of these environmental perturbations. Our profiles of $\delta^{44/40}Ca$ and $\delta^{13}C$ in Fig. 6 do not accord with any of the model outputs of Silva-Tamayo *et al.* (2018, Fig. 8).

A negative excursion of $\delta^{44/40}Ca_{cal}$ is not shown by our data for Peniche in the upper *semicelatum* to mid-*exaratum* interval, whether the data is corrected or uncorrected (Fig. 6). The profile of temperature-corrected $\delta^{44/40}Ca_{cal}$ shows a small positive excursion at the top of the *semicelatum 1* Subzone, which is the opposite of what is expected from ocean acidification. The detrended values of $\delta^{44/40}Ca_{cal}$ do not show any resolvable positive or negative excursion, unless it is a positive blip at the top of the *semicelatum 1* Subzone. A superficial similarity to Model B in Fig. 8 is seen in that the *exaratum* profile shifts to more negative values in $\delta^{13}C_{cal}$ and (possibly) a (small) positive excursion in $\delta^{44/40}Ca$ but, in Model B, the excursions are in phase and in our data they are out of phase. The failure of the isotopic profiles in Peniche to conform to any model in Fig. 8 applies whether the shift of $\delta^{13}C$ in Zone 2 to more negative (or less positive) values is interpreted as reflecting a specific forcing *e.g.* from volcanogenic CO_2, or is interpreted as reflecting nothing but a temporary relaxation of the forcing that was driving the positive isotope excursions of $\delta^{13}C$ in the Tenuicostatum and Bifrons Zones (McArthur 2007).

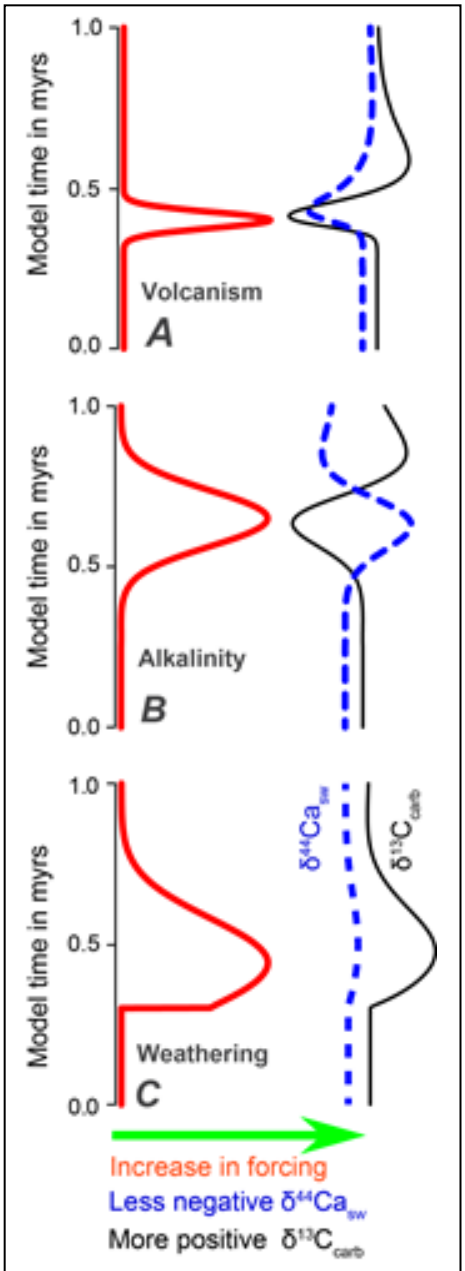

Fig. 8. Variations by $\delta^{44/40}Ca$ in seawater and $\delta^{13}C$ in carbonate sediment as a consequence of variations in three driving factors, as modelled by Silva-Tamayo *et al.* (2018).

Ocean acidification might explain the minimum in temperature-corrected $\delta^{44/40}Ca_{cal}$ at around 8 m in the section (Fig. 6b) but the minimum is not seen in detrended data (Fig. 6c) nor is seen in our profile of $\delta^{88/86}Sr_{cal}$. The minimum, if real, may be an artefact of the shortness of the section: a longer section might show a background value of 1.45 ‰ superimposed on which are two positive excursions at around 0 m and 12 m in the section – only a longer profile interval can resolve this issue.

Neither is ocean acidification needed to explain our profiles. Allowance must be made for condensation of strata in the interval 0 to 3 m (McArthur *et al.* 2020a), which accentuates the apparent rate of change of all chemical and isotopic profiles in that interval in Peniche: the *exaratum* Subzone of Yorkshire is also condensed relative to underlying and overlying strata (McArthur et al. 2000). When allowance is made for condensation at Peniche, values of $\delta^{44/40}Ca_{cal}$ show no more variation per Ma through

the interval of study, a period of between 1 and 3 myrs, than is seen through much of Phanerozoic time (de la Rocha and DePaolo 2000; Farkaš *et al.* 2007a,b).

Finally, if global warming, and so a hydrological cycle of greater intensity (more rain), was associated with LIP volcanism in the interval, more continental erosion would have resulted, with more sediment being supplied to the oceans, a scenario difficult to reconcile with hydrographic restriction and sediment starvation in many basins of northern Tethys at this time (Baroni *et al.* 2018; McArthur *et al.* 2000). Increased rainfall and erosion is also at odds with the suggestion that, at least in the terrestrial hinterland of the Cleveland Basin, conditions in *exaratum* times were warmer but drier than before or after (Slater *et al.* 2019).

4. Caveats

Interpretation of the records for Peniche is affected by several factors. The first is the shortness of the record, a problem that affects the interpretation of many Toarcian isotopic profiles. Without definition of a long-term trend that establishes a background trend (the baseline) for any variable (here, isotopic profiles through time), it is difficult or impossible to interpret changes in those profiles. We contend that the interval from mid *Semicelatum I* time through the lower *exaratum* Subzone (the supposed interval of acidification) does not show a negative excursion in either $\delta^{44/40}Ca_{cal}$ or $\delta^{88/86}Sr_{cal}$, but longer and more densely populated records would establish this point with greater confidence.

The second caveat is whether the use of a composite section is justified. The Cleveland Basin, in Yorkshire, the source of the Yorkshire belemnites, was hydrographically restricted for much, if not most, of *exaratum* time (McArthur *et al.* 2008; McArthur 2019), with euxinia extending into the photic zone (Schouten *et al.,* 2000; Wignall *et al.,* 2005; French *et al.* 2014). Nevertheless, ammonite faunas preserved in sediments of the *exaratum* Subzone in Yorkshire attest to an oxic surface layer. Sporadic benthic colonisation in Yorkshire (Caswell and Coe 2009, 2013) and in Germany (Röhl *et al.* 2001; Schmid-Röhl *et al.* 2002) by opportunistic bivalves testify to multiple oxygenation events affecting the entire water column, events possibly as brief as a single season (*ibid*). The Yorkshire belemnites, typically associated with hiatuses in sedimentation, probably migrated into the area during the brief episodes when the full water column was oxic; they record temperatures higher than samples from Peniche, but appear otherwise typical of Jurassic belemnites. The $^{87}Sr/^{86}Sr$ ratios of specimens from both localities are concordant (McArthur *et al.* 2020a) and the values of $\delta^{13}C$, Mg/Ca, and Sr/Ca in the Yorkshire belemnites are not obviously anomalous in comparison to belemnites from upper Pliensbachian and lower Toarcian strata at Peniche and elsewhere *e.g.* Spain (Rosales *et al.* 2004). The belemnites from Yorkshire fall on a correlation line

between $\delta^{44/40}$Ca and both Mg/Ca and temperature (Fig. 3a). Our use of a composite sample set therefore seems valid.

The third factor, is that our data have been acquired on two different belemnite families, and on brachiopods as well, although we emphasise that the brachiopods occur in Zone 3, the retreat phase of the mechanism driving change and so are of lesser importance to our arguments. Nevertheless, all three groups conform to a good correlation between $\delta^{44/40}$Ca and temperature, whilst $\delta^{88/86}$Sr appears to be independent of taxon, temperature, or Sr/Ca.

The final factor is the possibility that the salinity of seawater, and so its δ^{18}O, might have differed between Peniche and Yorkshire and so affect the temperature corrections we make that are based on $\delta^{18}O_{sw}$. We conducted a sensitivity analysis (Fig. S3) by varying the values of $\delta^{18}O_{sw}$ for Yorkshire only by up to ± 1 ‰ from our assumed value of −1 ‰ for an ice-cap-free world and examined the resulting changes to Figs. 3a and 6. Values of $\delta^{18}O_{sw}$ more positive than −1 ‰ flatten the profile of temperature-corrected $\delta^{44/40}$Ca, lessens but does not remove the positive excursion in the early part of Zone 2, and gives implausibly high palaeo-temperatures of up to 45 °C in Yorkshire. Values of $\delta^{18}O_{sw}$ more negative than −1 ‰ increase the positive anomaly in the early part of Zone 2, largely because the temperatures in Yorkshire are decreased and so the temperature corrections for Yorkshire are decreased. Values more negative than −1 ‰ for $\delta^{18}O_{sw}$ also seriously degrade the correlation between temperature and $\delta^{44/40}$Ca; from 0.81 at −1 ‰ to 0.69 at −2 ‰ (for details, see the Supplementary Information and Fig. S3).

Whatever data set is accepted (base-, temperature-corrected, or detrended), no profile of $\delta^{44/40}$Ca or $\delta^{88/86}$Sr shows a negative excursion in mid *semicelatum I* to *exaratum* time so the data do not support the presence of ocean acidification during this interval. This finding accords with the data of Müller *et al.* (2020), who provide a profile of δ^{11}B in brachiopod calcite through the Peniche section. Their sample contain up to 4% Al, and the samples they analysed for δ^{11}B contain up to 1.2% Al, possibly in a Mg-rich clay contaminant such as palygorskite (Fig. S4), with the samples most affected being in the dysoxic interval. In Fig. 9, their data are corrected for contamination by clays, based on the statistically significant correlation between Al concentration and δ^{11}B (Fig. S6). Given the need to correct for contamination, and the uncertainties of the analysis, with different samples from the same level differing in δ^{11}B by up to 1.4 ‰ (Supplementary Information of Müller *et al.* 2020) we contend that a flat profile is the most likely interpretation of the data; and that there are no convincing departures through the section of δ^{11}B from the mean value of δ^{11}B defined by the vertical pale-blue line in Fig 9. Since δ^{11}B is sensitive to the pH of seawater, the data of Müller *et al.* (2020) suggest that the pH of seawater did not change through the interval.

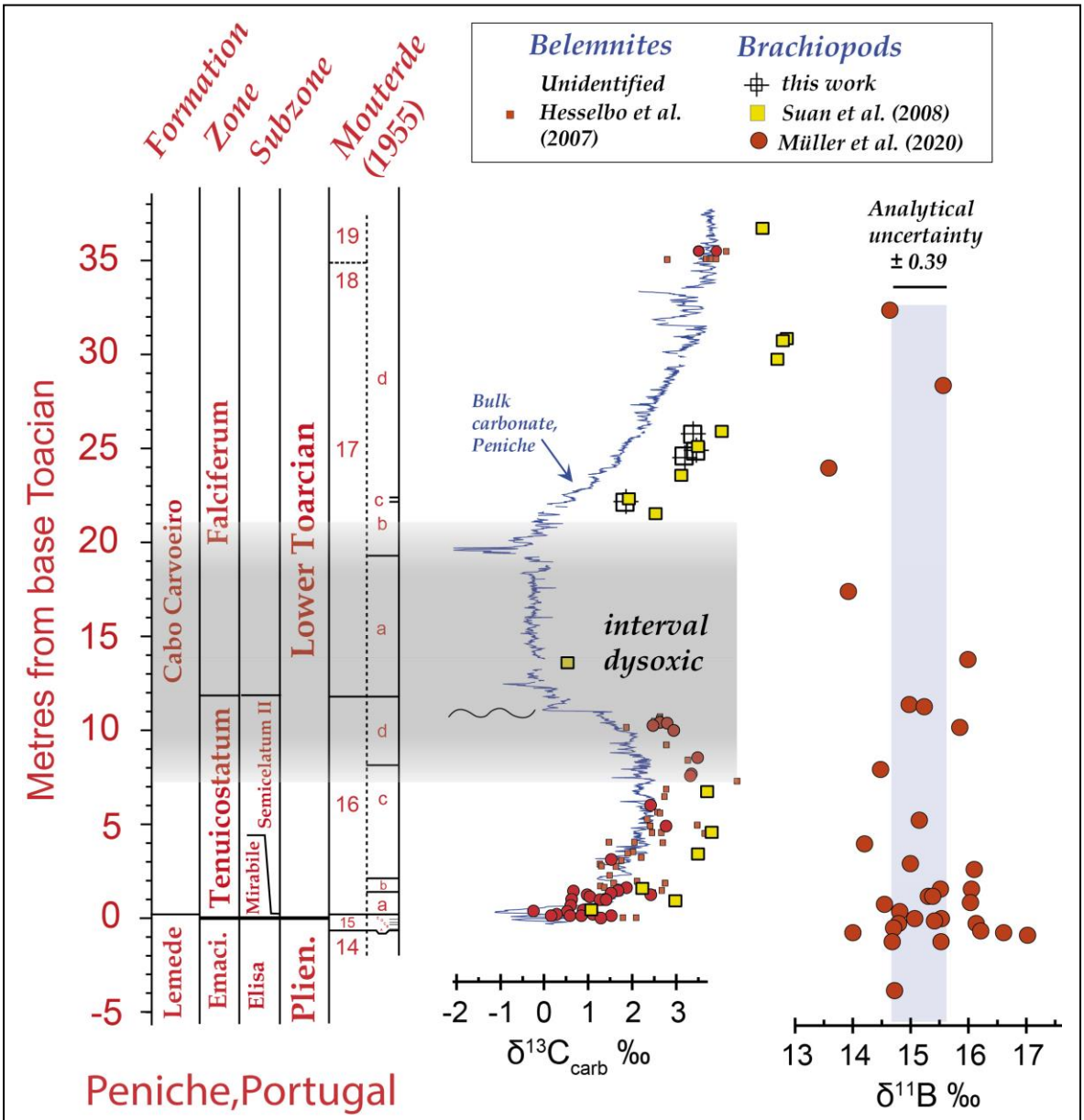

Fig. 9. Profiles of $\delta^{11}B$ in brachiopod calcite from Peniche; data from Muller *et al.* (2020), corrected for Al contamination (see Supplementray Information). Blue vertical lines is drawn at the mean values of corrected $\delta^{11}B$ and has a width equal to analytical uncertainty, calculated as the mean deviation from the means of 10 analyses of 5 pairs of samples from 5 different levels (mean 0.39 ‰, 2 s.d. = 0.58, n = 5).

5. The Mg/Ca palaeo-thermometer.

Values of Mg/Ca in pristine biogenic carbonate increase as the temperature of calcification increases, so Mg/Ca has been widely used as a palaeo-temperature proxy in foraminifera (Chave 1954; Lea 2014). Its application to belemnites has had limited success. In our belemnites, Mg/Ca correlates positively with temperature (Fig. 10) but the data are bimodal and scatter somewhat. Nevertheless, we contend that the bimodal distribution arises because the temperatures at which our belemnites calcified did not span the full range needed to make the distribution normal; we point

particularly to the facts that two Megateuthids from Peniche (133A, B) plot with the remaining Peniche samples, which are Passaloteuthids, whilst the lowest sample from Yorkshire stratigraphically, a Megateuthid, also plots with the Passaloteuthids from Peniche suggesting that, despite the bimodality, the correlation has meaning and is not just a co-incidental, two-point, correlation between Megateuthids on the one hand and Passaloteuthids on the other.

The palaeo-temperature equation given in Fig. 10 has uncertainties that are too large for the equation to be presently useful, or to prove it is linear. Nevertheless, Figs. 3a and 10 suggests that the temperature dependence of Mg/Ca in belemnites warrants further research in an effort to derive a better palaeo-temperature equation. Specific attention should be paid to the following. 1) analytical uncertainty; the analysis of Mg/Ca (and Sr/Ca) should be done by the ratio-intensity method of de Villiers (2002) or the methods of Schrag (1999) or Rosenthal (1999). Adoption of such rigorous methods will, for example, avoid the bias in the low % levels that can arise in AES from differing El/Ca in samples being compared to standards of fixed El/Ca.. 2) identification of analysed samples to at least family level and preferably species level so that species-specific effects can be isolated. 3) consistent sampling of the belemnite rostrum. Belemnites exhibit radial and longitudinal gradients in El/Ca, so where in a belemnite a subsample is taken is critical to acquisition of consistent data. 4) the magnitude of variations in Mg/Ca that arise from variations in calcification rate and their correction. 5) assessment of preservation. Only gross alteration can be detected by chemical analysis, so optical methods should be used as the primary means of evaluating the state of preservation of a sample.

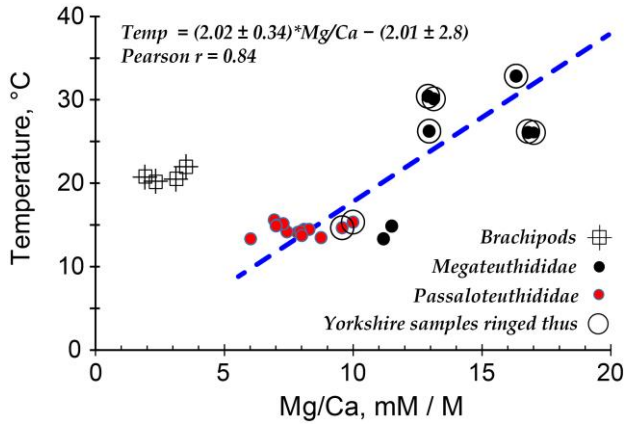

Fig. 10. Relation of Mg/Ca to temperature in belemnites. The bimodality is discussed in the text.

6. Conclusions

No negative excursion was found in $\delta^{44/40}Ca_{cal}$ or $\delta^{88/86}Sr_{cal}$ in belemnite or brachiopod calcite through the interval from the mid *semicelatum* Subzone to the end *exaratum* Subzone, an interval commonly termed the Toarcian oceanic anoxic event. It follows that ocean acidification postulated for the interval was not of a magnitude to disturb the Ca-isotopic composition of the ocean at the analytical resolution currently available.

Values of $\delta^{44/40}Ca$ in Passaloteuthididae belemnites, Megateuthididae belemnites, and

brachiopods of the species *Soaresirhynchia bouchardi*, show a positive correlation between $\delta^{44/40}Ca$ and temperature with a sensitivity of 0.020‰ increase per °C increase in temperature. For belemnites only, $\delta^{44/40}Ca$ correlates positively with Mg/Ca and Sr/Ca. Values of $\delta^{88/86}Sr_{cal}$ are independent of temperature and Sr/Ca. The Mg/Ca of belemnites of two families Passaloteuthididae and Megateuthididae correlate with temperature and define a palaeo-temperature equation for belemnites that takes the form $T°C = (2.02 \pm 0.34)*Mg/Ca - (2.01 \pm 2.8)$. The equation has uncertainties too large for present use and requires refinement through standardization of techniques for preparation and analysis.

Acknowledgements

We thank * anonymous reviewers for reviews that were helpful and constructive, and L.V. Duarte for assistance in the field.

Statement of Funding. This work was funded by grant from the Leverhulme Trust.

References:

Al-Khatib M. and Eisenhower A. 2017. Calcium and strontium isotope fractionation in aqueous solutions as a function of temperature and reaction rate; I. Calcite. *Geochim. Cosmochim. Acta*, **209**, 296–319.

Al-Suwaidi A.H., Angelozzi G.N., Baudin F., Damborenea SE. Hesselbo S.P., Jenkyns H.C., Manceñido M.O., Riccardi A.C. 2010. First record of the Early Toarcian Oceanic Anoxic Event from the Southern Hemisphere, Neuquen Basin, Argentina. *Jour. Geol. Soc. London,* **167(4)**, 633–636

Bailey T.R., Rosenthal Y., McArthur J.M., van de Schootbrugge B. and Thirlwall M.F. 2003. Paleoceanographic changes of the Late Pliensbachian–Early Toarcian interval: a possible link to the genesis of an Oceanic Anoxic Event. *Earth Planet. Sci. Letters*, **212**, 307–320.

Baroni I.R., Pohl A., van Helmond N.A.G.M., Papadomanolaki N.M., Coe A.L., Cohen A.S., van de Schootbrugge B., Donnadieu Y. and Slomp C.P. 2018. Ocean circulation in the Toarcian (Early Jurassic): a key control on deoxygenation and carbon burial on the European shelf. *Paleoceanography and Paleoclimatology*, **33**, 994–1012.

Bodin S., Mattioli E., Fröhlich S., Marshall J.D., Boutib L., Lahsini S. and Redfern J. 2010. Toarcian carbon isotope shifts and nutrient changes from the Northern margin of Gondwana (High Atlas, Morocco, Jurassic): palaeoenvironmental implications. *Palaeogeography, Palaeoclimatology, Palaeoecology*, **297**, 377–390.

Bradbury H. J. and Turchyn A. V. 2018. Calcium isotope fractionation in sedimentary pore fluids from ODP Leg 175: Resolving carbonate recrystallization. *Geochim.Cosmochim. Acta,* 236, 121–139.

Brazier J-M., Suan G., Tacail T., Simon L., Martin J.E., Mattioli E and Balter V. 2015. Calcium isotope evidence for dramatic increase of continental weathering during the Toarcian oceanic anoxic event (Early Jurassic). *Earth and Planetary Science Letters* 411, 164–176.

Black B.A., Elkins-Tanton L.T., Rowe M.C. and Peate I.U. 2012. Magnitude and consequences of volatile release from the Siberian Traps. *Earth Planet. Sci. Letters*, **317–318**, 363–373.

Böhm F., Eisenhauer A., Tang J., Dietzel M., Krabbenhöft A., Kisakürek B. and Horn C., 2012. Strontium isotope fractionation of planktic foraminifera and inorganic calcite. *Geochim. Cosmochim Acta*, **93**, 300–314.

Burgess S.D., Bowring S.A., Fleming T.H. and Elliot D.H. 2015. High-precision geochronology links the Ferrar large igneous province with early-Jurassic ocean anoxia and biotic crisis. *Earth Planet. Sci. Letters*, 415, 90–99.

Caswell B.A., Coe A.L. and Cohen A.S. 2009. New range data for marine invertebrate species across the early Toarcian (Early Jurassic) mass extinction. *Jour. Geol. Soc. London*, **166**, 859–872. doi: 10.1144/0016-76492008-0831.

Caswell B.A. and Coe A.L. 2013. Primary productivity controls on opportunistic bivalves during Early Jurassic oceanic deoxygenation. *Geology*, **41(11)**, 1163–1166.

Chave K.E. 1954. Aspects of the biogeochemistry of magnesium 1. Calcareous marine organisms. *Journal of Geology*, **62(3)**, 266–283.

Daëron M., Drysdale R.N., Peral M., Huyghe D., Blamart D., Coplen T.B., Lartaud F. and Zanchett, G. 2019. Most Earth-surface calcites precipitate out of isotopic equilibrium. *Nature Communications*, 10:429, doi.org/10.1038/s41467-019-08336-

Danise S., Twitchett R.J., Little C.T.S. and Clémence M-E. (2013). The impact of global warming and anoxia on marine benthic community dynamics: an example from the Toarcian (Early Jurassic). *PloS One*, **8(2)**, e56255.

De La Rocha C.L. and DePaolo D.J. 2000. Isotopic evidence for variations in the marine calcium cycle over the Cenozoic. *Science*, **289**, 1176–1178.

de Villiers S., Greaves M. and Elderfield H. 2002. An intensity ratio calibration method for the accurate determination of Mg/Ca and Sr/Ca of marine carbonates by ICP-AES. *Geochem. Geophys. Geosyst.*, **3**, 10.1029/2001GC000169.

DePaolo, D.J. 2011. Surface kinetic model for isotopic and trace element fractionation during precipitation of calcite from aqueous solutions. *Geochimica et Cosmochimica Acta*, 75(4), 1039–1056.

Dera G., Pellenard P., Neige P., Deconinck J-F., Pucéat E. and Dommergues J-L. 2009. Distribution of clay minerals in early Jurassic Peritethyan seas: palaeoclimatic significance inferred from multiproxy comparisons. *Palaeogeogr. Palaeoclimatol. Palaeoecol.*, 271(1–2), 39–51.

Duarte L.V., Silva R.L., Félix F., Comas-Rengifo M.J., Rocha R.B., Mattioli E., Paredes R., Filho J.G.M. and Cabral M.C. (2017). The Jurassic of the Peniche Peninsula (Portugal): scientific, educational and science popularization relevance (El Jurásico de la Península de Peniche (Portugal): relevancia científica, educativa y divulgativa). *Revista de la Sociedad Geológica de España*, **30(1)**, 55–70.

Duarte L.V, Comas-Rengifo M.J., Hesselbo S., Mattioli E., Suan G., (coordinators), Baker S., Cabral M.C., Correia V., García Joral F., Goy A., Reolid M., Rita P., Félix F., Paredes R., Pittet B. and Rocha R.B. 2018. The Toarcian Oceanic Anoxic Event at Peniche. An exercise in integrated stratigraphy - Stop 1.3. *In*: Duarte L.V. and Silva R. (Eds). Field Trip Guidebook: The TOAE in the Western Iberian Margin and its context within the Lower Jurassic evolution of the Lusitanian Basin. Second International Workshop on Toarcian Oceanic Anoxic Event, Coimbra,, Portugal, 2018.

Elmi S. 2007. Pliensbachian/Toarcian boundary: the proposed GSSP of Peniche (Portugal). *Ciências da Terra/Earth Sciences Journal*, **16,** 7–16.

Farkaš, J., Florian Böhm, Wallmann K., Blenkinsop J., Eisenhauer A., van Geldern R., Munnecke A., Voigt S., and Veizer J. 2007a. Calcium isotope record of Phanerozoic oceans: Implications for chemical evolution of seawater and its causative mechanisms. *Geochim.Cosmochim. Acta*, **71(21)**, 5117–5134.

Farkaš, J., Buhl, D., Blenkinsop, J. and Veizer, J. 2007b. Evolution of the oceanic calcium cycle during the late Mesozoic: Evidence from $\delta^{44/40}$Ca of marine skeletal carbonates. *Earth Planet. Sci. Letters*, **253(1)**, 96–111.

Fietzke, J. and Eisenhauer, A. 2006. Determination of temperature-dependent stable strontium isotope (^{88}Sr/^{86}Sr) fractionation via bracketing standard MC-ICP-MS. *Geochem. Geophys. Geosyst.*, **7**, Q08009, doi:10.1029/2006GC001243

French, K.L., Sepúlveda J., Trabucho-Alexandre J., Gröcke D.R. and Summons R.E. 2014. Organic geochemistry of the earlyToarcian oceanic anoxic event in Hawsker Bottoms,Yorkshire, England. Earth and Planetary Science Letters 390, 116–127.

Guex J., Pilet S., Müntener O., Bartolini A., Spangenberg J., Schoene B., Sell B. and Schaltegger U., 2016. Thermal erosion of cratonic lithosphere as a potential trigger for mass-extinction. *Sci. Reports*, **6**, 23168.

Gussone N., Böhm F., Eisenhauer A., Dietzel M., Heuser A., Teichert B.M.A., Reitner J., Wörheide G., and Dullo W.-C. 2005. Calcium isotope fractionation in calcite and aragonite. *Geochimica et Cosmochimica Acta*, 69(18), 4485–4494.

Gussone N. and Heuser A. 2016. Biominerals and biomaterial. In: Gussone N., Schmitt A.-D., Heuser A., Wombacher F., Dietzel M., Tipper E. and Schiller M. (Eds.), Calcium Stable Isotope Geochemistry. Springer Heidelberg (260pp).

Hallam A. 1986. The Pliensbachian and Tithonian extinction events. *Nature*, **31**9, 765–768.

Harries P.J. and Little C.T. 1999. The early Toarcian (Early Jurassic) and the Cenomanian–Turonian (Late Cretaceous) mass extinctions: similarities and contrasts. *Palaeogeography, Palaeoclimatology, Palaeoecology*, **154**, 39–66.

Hays P.D. and Grossman E.L. 1991. Oxygen isotopes in meteoritic calcite cements as indicators of continental paleoclimate. *Geology*, **19(5)**, 441–444.

Hermoso M., Minoletti F. Le Callonnec L., Jenkyns H.C., Hesselbo S.P., Rickaby R.E.M., Renard, M., Rafélis M. and Emmanuel L. 2009. Global and local forcing of Early Toarcian seawater chemistry: a comparative study of different paleoceanographic settings (Paris and Lusitanian basins). *Paleoceanography*, **24**, PA4208, doi:10.1029/2009PA001764.

Hesselbo S.P., Gröcke, D.R., Jenkyns, H.C., Bjerrum, C.J., Farrimond, P., Morgans Bell, H.S. and Green, O.R. 2000. Massive dissociation of gas hydrate during a Jurassic oceanic anoxic event, *Nature*, **406**, 392–395.

Hesselbo S.P., Jenkyns H.C., Duarte L.V. and Oliveira L.C.V. 2007. Carbon-isotope record of the Early Jurassic (Toarcian) Oceanic Anoxic Event from fossil wood and marine carbonate (Lusitanian Basin, Portugal). *Earth Planet. Sci. Letters*, **253**, 455–470.

Howarth M.K. 1962. The Jet Rock series and the Alum Shale series of the Yorkshire coast. *Proceedings of the Yorkshire Geological Society*, **33(4)**, 381–422.

Howarth M.K. 1991–1992. The ammonite family Hildoceratidae in the Lower Jurassic of Britain. *Monographs of the Palaeontographical Society*, London: 200pp, 38pl.

Ivanov, A.V., Meffre, S., Thompson, J., Corfu, F., Kamenetsky, V.S., Kamenetsky, M.B. and Demonterova, E.I. 2017. Timing and genesis of the Karoo-Ferrar large igneous province: new high precision U-Pb data for Tasmania confirm short duration of the major magmatic pulse. *Chemical Geology*, *455*, 32–43.

Jost A.B., Bachan A., van de Schootbrugge B., Brown S.T., DePaolo D.J. and Payne J.L. 2017. Additive effects of acidification and mineralogy on calcium isotopes in Triassic/Jurassic boundary limestones. *Geochemistry, Geophysics, Geosystems*, **18(1)**, 113–124.

Jourdan, F., Féraud, G., Hervé, B., Kampunzu, A.B., Tshoso, G., Watkeys, M.K. and Gall, B.L. 2005. Karoo large igneous province: Brevity, origin, and relation to mass extinction questioned by new $^{40}Ar/^{39}Ar$ age data. *Geology*, **33(9)**, 745–748.

Jourdan, F., Féraud, G., Bertrand, H. and Watkeys, M.K. 2007. From flood basalts to the inception of oceanization: example from the 40Ar/39Ar high-resolution picture of the Karoo large igneous province. *Geochem. Geophysics Geosystems*, **8(2)**, Q02002, doi:10.1029/2006GC001392

Jourdan, F., Féraud, G., Bertrand ,H., Watkeys, M.K. and Renne, P.R. 2008. The $^{40}Ar/^{39}Ar$ ages of the sill complex of the Karoo large igneous province: implications for the Pliensbachian-Toarcian climate change. *Geochemistry, Geophysics, Geosystems*, **9(6)**, Q06009.

Kemp D.B., Coe A.L., Cohen A.S., Schwark L. 2005. Astronomical pacing of methane release in the Early Jurassic period. *Nature*, **437**, doi:10.1038/nature04037.

Kemp D.B. and Izumi K. 2014. Multiproxy geochemical analysis of a Panthalassic margin record of the early Toarcian oceanic anoxic event (Toyora area, Japan). Palaeogeog. Palaeoclimatol, Palaeoecol, 414, 332–341.

Kisakürek B., Eisenhauer A., Böhm F., Hathorne E.C. and Erez J. 2011. Controls on calcium isotope fractionation in cultured planktic foraminifera, *Globigerinoides ruber* and *Globigerinella siphonifera*. *Geochim. Cosmochim. Acta*, **75**, 427–443.

Krabbenhöft A., Fietzke J., Eisenhauer A., Liebetrau V., Böhm F. and Vollstaedt H. 2009. Determination of radiogenic and stable strontium isotope ratios ($^{87}Sr/^{86}Sr$; $\delta^{88}/^{86}Sr$) by thermal ionization mass spectrometry applying an $^{87}Sr/^{84}Sr$ double spike. *Journal of Analytical Atomic Spectrometry*, **24(9)**, 1267–1271.

Küspert W. 1982. Environmental changes during oil shale deposition as deduced from stable isotope ratios. In *Cyclic and event stratification* (pp. 482–501). Springer, Berlin, Heidelberg.

Lea D.W. 2014. Elemental and isotopic proxies of past ocean temperatures. Treatise of Geochemistry, 2nd Edition. Elsevier, 2014: http://dx.doi.org/10.1016/B978-0-08-095975-7.00614-8.

Li Q., Thirlwall M. and Müller W. 2016. Ca isotopic analysis of laser-cut microsamples of (bio) apatite without chemical purification. *Chem. Geol.* **422**, 1–12.

Little C.T.S. and Benton M.J. 1995. Early Jurassic mass extinction: a global long-term event. *Geology*, **23(6)**, 495–498.

McArthur J.M., Donovan D.T., Thirlwall M.F., Fouke B.W. and Mattey D. 2000. Strontium isotope profile of the early Toarcian (Jurassic) oceanic anoxic event, the duration of ammonite biozones, and belemnite palaeotemperatures. *Earth Planet. Sci. Letters*, **179**, 269–285.

McArthur J.M. 2007. Comment on "Carbon-isotope record of the Early Jurassic (Toarcian) Oceanic Anoxic Event from fossil wood and marine carbonate (Lusitanian Basin, Portugal)" by Hesselbo S., Jenkyns H.C., Duarte L.V. and Oliveira L.C.V. *Earth and Planetary Science Letters* **259**, 634–639.

McArthur J.M., Algeo T.J., Van de Schootbrugge B., Li Q. and Howarth R.J. 2008. Basinal restriction, black shales, Re-Os dating, and the Early Toarcian (Jurassic) oceanic anoxic event. *Paleoceanography*, **23(4)**. PA4217, doi:10.1029/2008PA001607.

McArthur, J.M. 2019. Early Toarcian black shales: a response to an oceanic anoxic event or anoxia. in marginal basins? *Chem. Geol.*, **522**, 71–83.

McArthur J.M., Page K, Duarte L.V., Thirlwall M.F., Li Q. and Weis R. 2020a. Sr-isotope

stratigraphy ($^{87}Sr/^{86}Sr$) of the lowermost Toarcian of Peniche, Portugal, and its relation to ammonite zonations. *Newsletters on Stratigrphy*, 53(3), 297–312. DOI: 10.1127/nos/2019/0492.

McConnaughey T. 1989. ^{13}C and $^{18}0$ isotopic disequilibrium in biological carbonates: I. Patterns *Geochim. Cosmochim. Acta*, **53**, 151–162.

Moulin M., Fluteau F., Courtillot V., Marsh J., Delpech G., Quidelleur X. and Gérard M. 2017. Eruptive history of the Karoo lava flows and their impact on early Jurassic environmental change. *J. Geophys. Res. Solid Earth*, **122**, 738–772.

Mouterde R. 1955. Le Lias de Peniche. Direcção general de minas e Serviçios geológicos.

Mouterde R. 1967. Le Lias du Portugal: vue d'ensemble et division en zones. *Comun. Serv. Geol. Portugal*, **52**, 209–226.

Müller M.N., Krabbenhöft A., Vollstaedt H., Brandini F.P., Eisenhauer A. 2018. Stable isotope fractionation of strontium in coccolithophore calcite: Influence of temperature and carbonate chemistry. *Geobiology*, **16**, 297–306.

Müller T., Jurikova H., Gutjahr M., Tomašových A., Schlög J., Liebetrau V., Duarte L.V., Milovský R., Suan G., Mattioli E., Pittet B and Anton Eisenhauer. 2020. Ocean acidification during the early Toarcian extinction event: evidence from boron isotopes in brachiopods. *Geology*, 48, https://doi.org/10.1130/G47781.1.

Nägler T.F., Eisenhauer A., Müller A., Hemleben C. and Kramers J. 2000. The $\delta^{44}Ca$-temperature calibration on fossil and cultured *Globigerinoides sacculifer*: new tool for reconstruction of past sea-surface temperatures. *Geochem. Geophys. Geosyst*., **1**, 2000GC0000091.

Nielsen L.C., Druhan J.L., Yang W., Brown S.T. and DePaolo D.J. 2012. Calcium Isotopes as Tracers of Biogeochemical Processes. *In*: Baskaran M. (eds) Handbook of Environmental Isotope Geochemistry. Advances in Isotope Geochemistry. Springer, Berlin, Heidelberg.

Page K.N. 2004. A sequence of biohorizons for the Subboreal Province Lower Toarcian in Northern Britain and their correlation with a Submediterranean Standard. *Rivista Italiana di Paleontologia e Stratigrafia*, **110**, 109–114.

Pálfy, J. and Smith, P.L. 2000. Synchronony between Early Jurassic extinction, oceanic anoxic event, and the Karoo–Ferrar flood basalt volcanism. *Geology*, **28**, 747–750.

Payne, J.L., Turchyn, A.V., Paytan, A., DePaolo, D.J., Lehrmann, D.J., Yu, M. and Wei, J., 2010. Calcium isotope constraints on the end-Permian mass extinction. *Proceedings of the National Academy of Sciences*, **107(19)**, 8543–8548.

Percival L.M.E., Cohen A.S., Davies M.K., Dickson A.J., Hesselbo S.P., Jenkyns H.C., Leng M.J., Mather T.A. 2016. Osmium isotope evidence for two pulses of increased continental weathering linked to Early Jurassic volcanism and climate change. *Geology*, **44(9)**, 759–762.

Pittet B., Suan G., Lenoir F., Duarte L.V., and Mattioli L.V. 2014. Carbon isotope evidence for sedimentary discontinuities in the lower Toarcian of the Lusitanian Basin (Portugal): Sea level change at the onset of the Oceanic Anoxic Event. *Sed. Geol.*, **303**, 1–14.

Raup, D. M. and Sepkoski, J.J. Jr. 1986. Periodic extinctions of families and genera. *Science*, **231**, 833–836.

Reynard, L.M., Henderson, G.M. and Hedges, R.E.M. 2010. Calcium isotope ratios in animal and human bone. *Geochim. Cosmochim. Acta*, **74(13)**, 3735–3750.

Rocha, R. B. de, Mattioli, E., Duarte, L. V., Pittet, B., Elmi, S., Mouterde, R., Cabral, M.-C., Comas-Rengifo, M.-J., Gómez, J.J., Goy, A., Hesselbo, S.P., Jenkyns, H.C., Littler, K., Mailliot, S., Luiz, Oliveira, L., C., Veiga, de, 10, Osete, M.-L., Perilli, N., Pinto, S., Ruget, C. and Suan, G. 2016. Base of the Toarcian Stage of the Lower Jurassic defined by the Global Boundary

Stratotype Section and Point (GSSP) at the Peniche section (Portugal). *Episodes*, **39(3)**, 460–481.
Röhl, H.-J., Schmid-Röhl, A., Oschmann, W., Frimmel, A., Schwark, L., 2001. The Posidonia Shale (lower Toarcian) of SW Germany: an oxygen depleted ecosystem controlled by sealevel and palaeoclimate. *Palaeogeogr. Palaeoclimatol. Palaeoecol.* **169**, 273–299.
Rosales, I., Quesada, S. and Robles, S. 2004. Paleotemperature variations of Early Jurassic seawater recorded in geochemical trends of belemnites from the Basque-Cantabrian basin, northern Spain. *Palaeogeog. Palaeoclimatol. Palaeoecol*., **203**, 253–275.
Rosenthal Y. , Field M.P. and Sherrell R.M. 1999. Precise determination of Element/Calcium ratios in calcareous samples using sector field inductively coupled plasma mass spectrometry. *Anal. Chem.*, **71**, 3248–3253.
Schmidt, A., Skeffington, R.A., Thordarson, T., Self S., Forster, P.M., Rap A., Ridgwell, A., Fowler, D., Wilson, M., Mann, G.W., Wignall, P.B. and Carslaw, K.S. 2016. Selective environmental stress from sulphur emitted by continental flood basalt eruptions. *Nature Geoscience*, **9**, 77–82.
Schmid-Röhl, A., Röhl, H., Oschmann, J.W., Frimmel, A., Schwark, L., 2002. Palaeoenvironmental reconstruction of Lower Toarcian epicontinental black shales (Posidonia shale, SW Germany): global versus regional control. *Geobios,* **35**, 13–20.
Schouten S., Van Kaam-Peters H.M.E., Rijpstra W.I.C., Schoell M., Sinninghe Damsté J.S., 2000. Effects of an oceanic anoxic event on the stable carbon isotopic composition of Early Toarcian carbon. *Am. J. Sci.* **300**, 1–22.
Schrag D.P. 1999. Rapid analysis of high-precision Sr/Ca ratios in corals and other marine carbonates. *Paleoceanography*, **14**, 97–102.
Silva-Tamayo J.C., Lau K.V., Jost A.B., Payne J.L., Wignall P.B., Newton R.J., Eisenhauer A., Depaolo D.J., Brown S., Mahe, K. and Lehrmann D.J., 2018. Global perturbation of the marine calcium cycle during the Permian-Triassic transition. *Bulletin*, *130*(7–8), 1323–1338.
Slater S.M., Twitchett R.J., Danise S. and Vajda V. 2019. Substantial vegetation response to Early Jurassic global warming with impacts on oceanic anoxia. *Nature Geoscience*, *12*(6), p.462.
Stoll H. M. and Schrag D. P. 2000. Coccolith Sr/Ca as a new indicator of coccolithophorid calcification and growth rate. *Geochem., Geophys., Geosystems*., **1**, 1–24.
Suan G., Mattioli E, Pittet B., Mailliot S. and Lécuyer C. 2008. Evidence for major environmental perturbation prior to and during the Toarcian (Early Jurassic) oceanic anoxic event from the Lusitanian Basin, Portugal. *Paleoceanography*, PA1202, doi:10.1029/2007PA001459, 14 pp.
Suan G., Mattioli E., Pittet B., Lécuyer C., Suchéras-Marx B., Duarte L.V., Philippe M., Reggiani L. and Martineau F. 2010. Secular environmental precursors to Early Toarcian (Jurassic) extreme climate changes. *Earth Planet. Sci. Letters,* **290**, 448–458.
Tang J., Dietzel M., Böhm F., Köhler S. J. and Eisenhauer A. 2008. Sr^{2+}/Ca^{2+} and $^{44}Ca/^{40}Ca$ fractionation during inorganic calcite formation: II. Ca isotopes. *Geochim. Cosmochim. Acta*, **72**, 3733–3745.
Thierry J. and Barrier E. 2000. Middle Toarcian. *In*: Atlas Peri-Tethys. Palaeogeographical Maps. Dercourt, J., Gaetani, M.E.A J. Dercourt, M. Gaetani, B. Vrielynck, E. Barrier, B. Biju-Duval, M.F. Brunet, J.P. Cadet, S. Crasquin and M. Sandulescu (Editors), Paris.
Uchikawa J. and Zeebe R.E. 2012. The effect of carbonic anhydrase on the kinetics and equilibrium of the oxygen isotope exchange in the CO_2–H_2O system: implications for $\delta^{18}O$ vital effects in biogenic carbonates. *Geochim. Cosmochim Acta*, **95**, 15–34.
Ullmann C.V. and Pogge von Strandmann P.A.E. 2017. The effect of shell secretion rate on Mg/Ca

and Sr/ Ca ratios in biogenic calcite as observed in a belemnite rostrum. *Biogeosciences*, 14, 89–97.

Vollstaedt H., Eisenhauer A., Wallmann K., Böhm F., Fietzke J., Liebetrau V., Krabbenhöft A., Farkaš J., Tomašých A., Raddatz J. and Veizer J. 2014. The Phanerozoic $\delta^{88/86}$Sr record of seawater: new constraints on past changes in oceanic carbonate fluxes. *Geochimica et Cosmochimica Acta*, **128**, 249–26.

von Allmen K., Nägler T.F., Pettke T., Hippler D., Griesshaber E., Logan A., Eisenhauer A. and Samankassou E. 2010.Stable isotope profiles (Ca, O, C) through modern brachiopod shells of *T. septentrionalis* and *G. vitreus*: implications for calcium isotope paleo-ocean chemistry.

Watkins J.M., Nielsen L/C.., Ryerson F.J. and DePaolo D.J. 2013. The influence of kinetics on the oxygen isotope composition of calcium carbonate. *Earth Planet. Sci. Letters*, **375**, 349–360.

Wignall, P.B., Newton, R.J. and Little, C.T.S. 2005. The timing of paleoenvironmental change and cause-and-effect relationships during the Early Jurassic mass extinction in Europe. *Am. J. Sci*. **305**, 1014–1032.

Xu W., Ruhl M., Jenkyns H.C., Hesselbo S.P., Riding J.B., Selby D., Naafs B.D.A., Weijers J.W.H., Pancost R.D., Tegelaar E.W. and Idiz E.F. 2017. Carbon sequestration in an expanded lake system during the Toarcian Oceanic Anoxic Event. *Nat. Geosci.* **10**, 129–134.

Supplementary Information

Testing with $\delta^{44/40}$Ca and $\delta^{88/86}$Sr for ocean acidification during the early Toarcian.

Q. Li[1,], J.M. McArthur[1,2,], M.F. Thirlwall[1], A.V. Turchyn[3], K. Page[4], H.J. Bradbury[3], R. Weis[5] and D. Lowry[1]*

3. Earth Science, Royal Holloway University of London, Egham Hill, Egham, UK, TW20 0EX
2. Department of Earth Sciences, UCL, Gower Street, London WC1E 6BT, UK
3. Department of Earth Sciences, University of Cambridge, Cambridge, UK
4. University of Exeter, Penryn Campus, Penryn, Cornwall TR10 9FE,UK.
5. Palaeontological Department, National Museum of Natural History, 25 rue Münster, L-2160, Luxembourg, Grand-duchy of Luxembourg.

**Present address, Nu Instruments, Clywedog Road South, Wrexham, UK, LL13 9XS*
2. Corresponding author email: j.mcarthur@ucl.ac.uk

4.1. Sample preservation

Coherent trends of multiple palaeo-proxies through the studied interval, discussed briefly below, attest to the good preservation of the samples. The Yorkshire belemnites analyzed here are those used to define the marine-$^{87}Sr/^{86}Sr$ curve through the Toarcian and the later part of the Pliensbachian (McArthur *et al.* 2000). Palaeoclimatic change through the same interval was examined by Bailey *et al.* (2003) using Sr/Ca, Mg/Ca, Li/Ca and $\delta^{18}O$ from the same, and other, belemnites. The Peniche belemnites analyzed here are those used to prove the synchroneity of ammonite correlations between Peniche and Yorkshire (McArthur *et al.* 2020a); the concordance of $^{87}Sr/^{86}Sr$ data between Peniche and Yorkshire provides compelling evidence of good preservation of analyzed samples. Discussions of preservation were presented in those papers. A more detailed study of Yorkshire samples in thin-section was made by McArthur *et al.* (2007) and a more comprehensive account of belemnite preservation can be found in Saelen *et al.* (1989), Podlaha *et al.* (1998), and McArthur *et al.* (2020b).

We assessed the degree of preservation/alteration of our samples by visual inspection of whole samples with the naked eye and with a hand lens, and inspection of fragmented samples by eye under the binocular microscope. For belemnites in hand specimen, the diagnostic features of good preservation are clarity of calcite and a brown colour in the range light to dark. The concentric rings typically seen in transverse section, and often termed 'growth rings', are faint or absent in well preserved belemnites. These bands are, in fact, rings caused by diagenetic alteration (Saelen *et al.* 1989). Alteration in belemnites is patchy, so even where alteration rings are abundant, the fragmented sample usually yields unaltered material. In fragmented samples picked for analysis, the diagnostic features of good preservation are a radial fabric, transparency, and little or no colour (Fig. S1). For fragmented brachiopods, the diagnostic features of good preservation are a readiness of the sample to flake into thin sheets, and a readiness of those sheets to disintegrate into lath-like crystallites of uncoloured, clear, calcite (Fig. S1). Our samples conform to these criteria.

We have not used trace-element composition, nor stable-isotope criteria, to assess alteration as such methods show alteration only after it is apparent to the naked eye in hand–specimen and under the microscope (McArthur *et al*. 2007; 2020a,b). Nevertheless, we note that the concentrations of

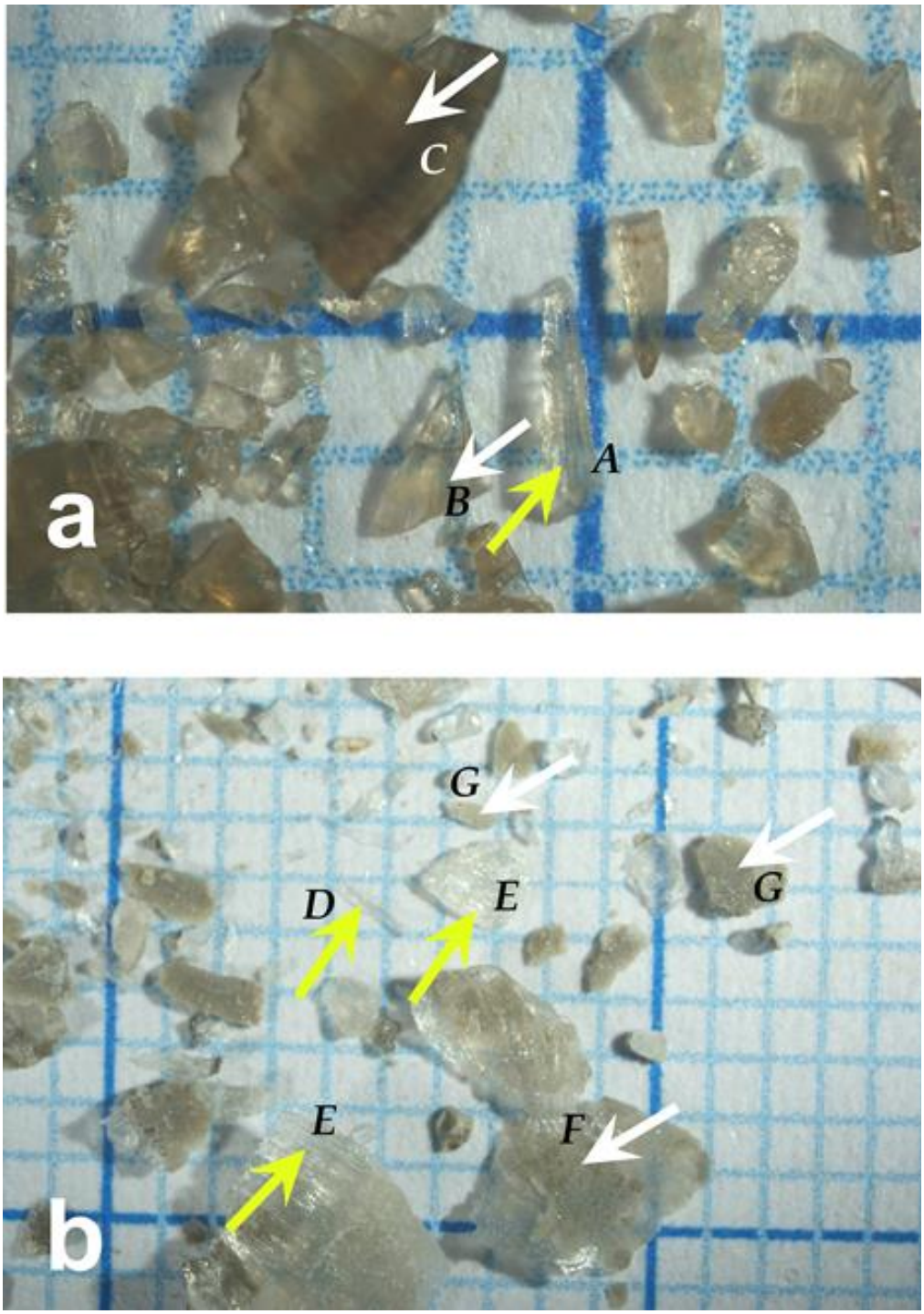

Fig. S1. Photomicrographs of fragments of a) belemnite 963 and b) brachiopod 9.65 m. White arrows point to altered fragments, yellow arrows point to unaltered fragments. Squares are 1 mm on a side. A, a fragment of pristine belemnite showing clear calcite with a strong radial fabric (oriented N-S); B, a triangular fragment in which pristine calcite (upper 30%) is separated from slightly altered calcite (lower 70%) by a black band that is interpreted to be organic matter. C, altered, cloudy, calcite from close to the belemnite exterior; useless for most chemical study. D, pristine crystallite of clear, pristine, calcite. E, foliated sheets of bundled crystallites of clear, pristine, calcite that flake to give thinner sheets and individual crystallites. F, foliated sheets of calcite in which the uppermost sheet is partly altered and cloudy. The upper sheet was easily flaked off from the underlying pristine calcite. G, altered calcite, the right-hand fragment being more altered than the left-hand fragment; both are useless for most chemical study.

860

Ca, Sr, Mg, and Na, and values of $\delta^{18}O$, in our samples (Table 1) are within the range of well-preserved biogenic calcites reported in the literature (*e.g.* Brand and Veizer 1980, 1981; Podlaha *et al*. 1998; *et seq.*); the Ba concentrations are ≤ 17 ppm with only 3 samples > 6 ppm; these low concentrations indicate good preservation in the sub-samples analyzed (McArthur *et al*. 2007). Concentrations of Mn are < 20 ppm excepting one sample containing 43 ppm and Fe concentrations exceed 100 ppm in only two samples; these higher Fe and Mn concentrations can be attributed to oxides deposited on crystal surfaces.

Correlation of C and O isotopes in samples

The positive correlation between base-$\delta^{44/40}Ca_{cal}$ and temperature (Fig. 3a) might be interpreted as suggesting that isotope fractionation of oxygen into belemnites is controlled by kinetic isotope fractionation, not equilibrium isotope fractionation (McConnaughey 1989; Watkins *et al.* 2013; Daëron *et al.* 2019). Values of $\delta^{18}O$ do not correlate with $\delta^{13}C$ (Fig. S2, below) as would be expected were kinetic isotope-effects influencing oxygen isotope compositions (see also Uchikawa and Zeebe 2012), so we discount kinetic isotope fractionation as significant either in generating the correlation seen in Fig. 3a, or as a contributor to the scatter in Fig. 3a.

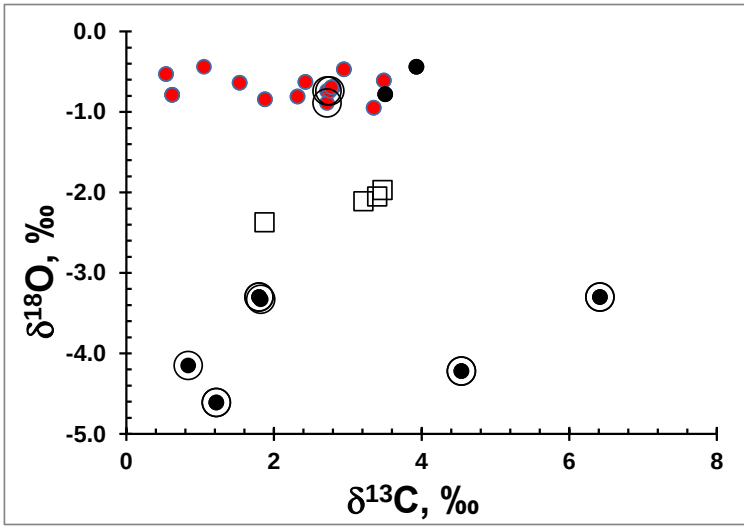

Fig. S2. Cross-plot of $\delta^{13}C$ *v* $\delta^{18}O$ for belemnites and brachiopods from Peniche, showing no relation between or within taxanomic groups

Sensitivity Analysis

The profiles of $\delta^{44/40}$Ca against stratigraphic level show a positive excursion in Zone 2 (Figs. 2, 6). The excursion occurs in raw data and in data corrected for temperature using a value of $\delta^{18}O_{sw}$ = −1 ‰. Here we show in Fig. S3 the effect (*cf.* Figs 3 and 6) of using alternate values of $\delta^{18}O_{sw}$ of +1‰ and −2‰ for seawater in Yorkshire whilst maintaining a value of −1‰ for Peniche. Other values can be interpolated or extrapolated from these values. Whatever values are chosen, the positive excursion in $\delta^{44/40}$Ca remains in Zone 2.

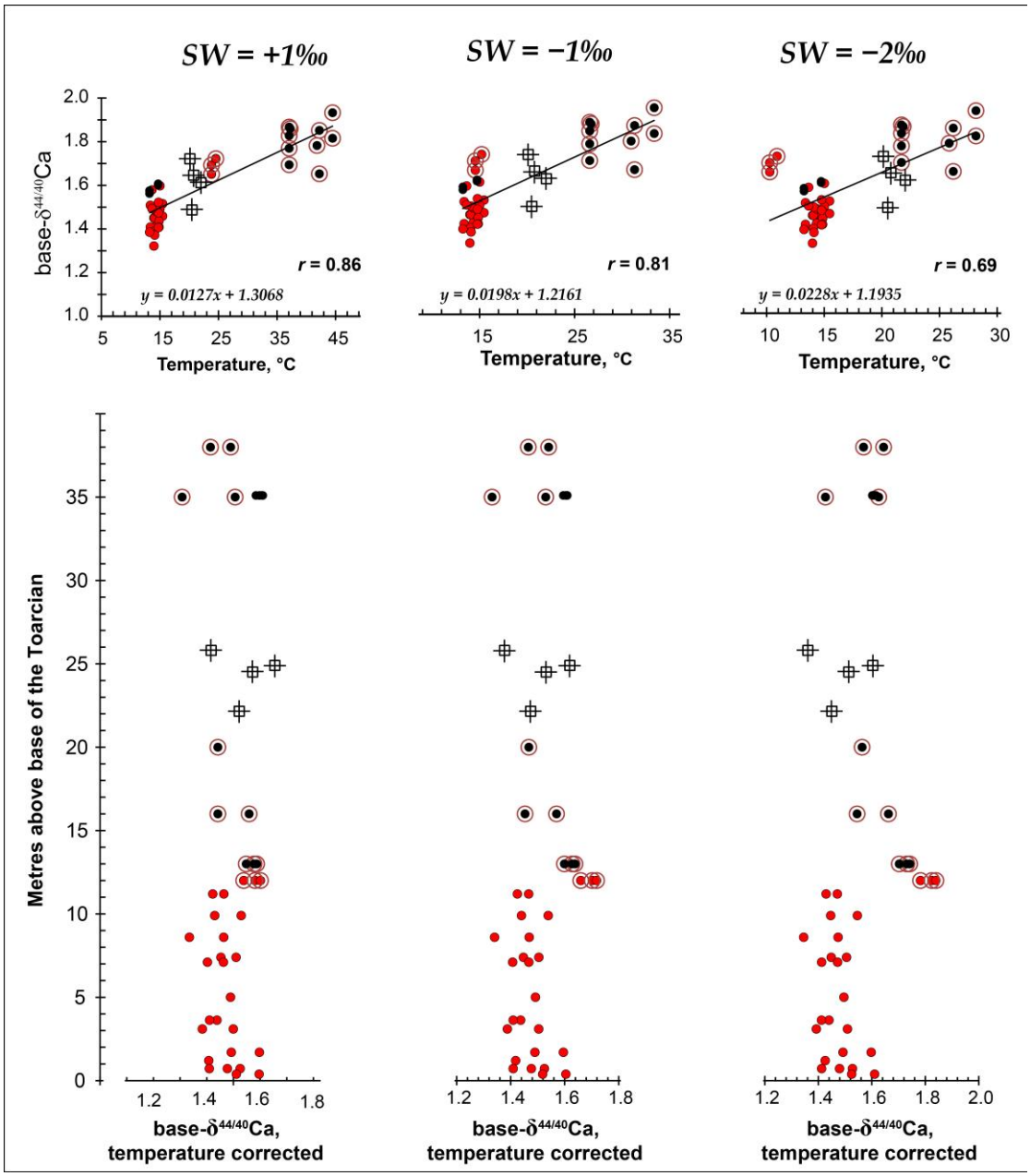

Fig. S3. Effect of differing values of $\delta^{18}O_{sw}$ on the temperature dependence of $\delta^{44/40}$Ca (as shown in Fig. 3a; upper three diagrams) and on the stratigraphic profile of $\delta^{44/40}$Ca (as shown in Fig. 6; lower three diagrams). Symbols as on previous figures.

Data of Müller *et al.* (2020), M20 hereinafter.

Sample Preservation.

The samples of M20 contain up to 4% Al (their Supplementary Information). Concentrations of Mg correlate strongly with concentrations of Al in many samples (Fig. S4), suggesting the presence of a contaminant phase containing both Mg and Al; possibly palygorskite or sepiolite that has precipitated between calcite crystallites as the organic matrix of the brachiopod shells decayed during early diagenesis. The presence of such a contaminant phase (others may not have been identified) suggests that the samples are not well preserved. This conclusion is confirmed by the excessively high values of $^{87}Sr/^{86}Sr$ of all but two samples, relative to expected values (Fig. S5). Furthermore, concentrations of Al correlate with $\delta^{11}B$ (Fig. S6). The correlation in Fig. 6 has been used to correct the values of $\delta^{11}B$ plotted in Fig. 9 for the effects of the contamination by Al.

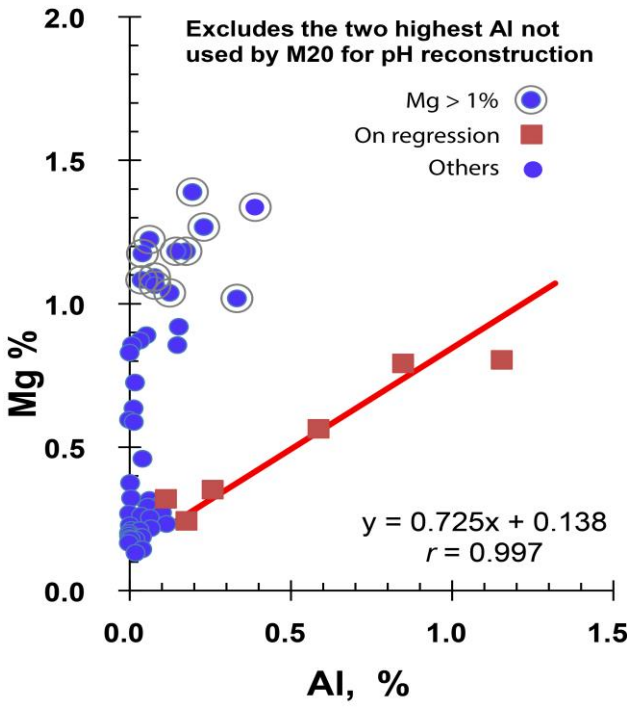

Fig. S4. Relation of Al to Mg in the samples of M20 analysed for $\delta^{11}B$. Red squares denote samples in which Mg and Al correlated most strongly. Two further samples fall exactly on the red regression line, contain up to 4% Al, but were not used for pH reconstruction by M20.

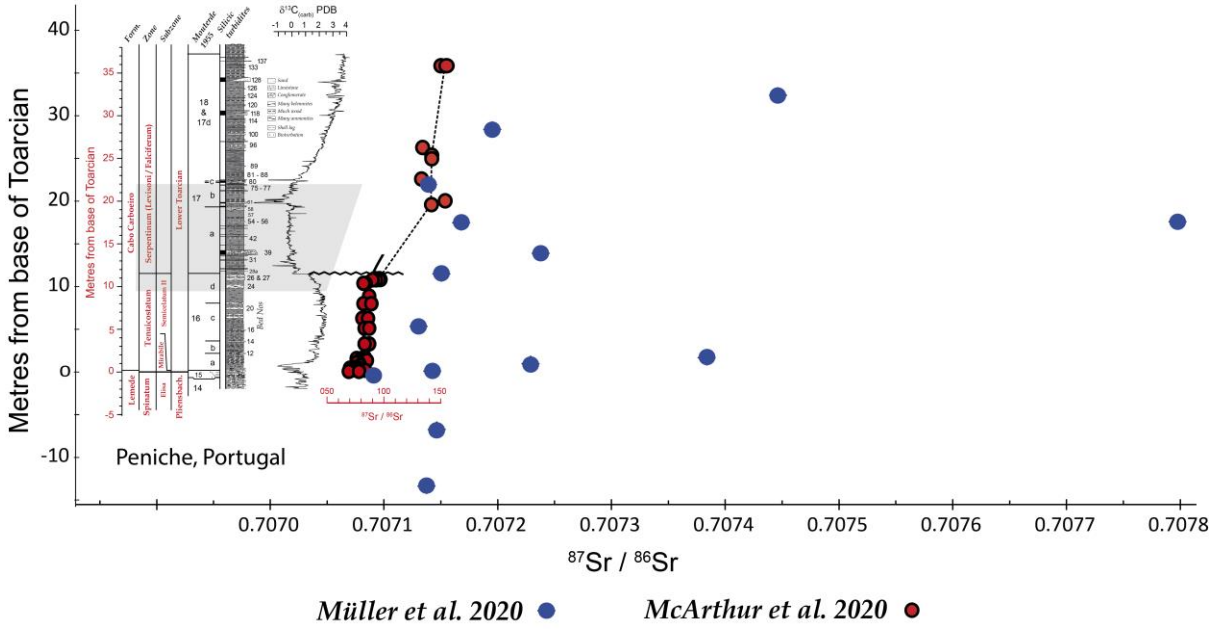

Fig. S5. Comparison of $^{87}Sr/^{86}Sr$ profiles for Peniche from M20 and from McArthur *et al.* (2020), with axes for stratigraphic level and for $^{87}Sr/^{86}Sr$ that are common to both data sets.

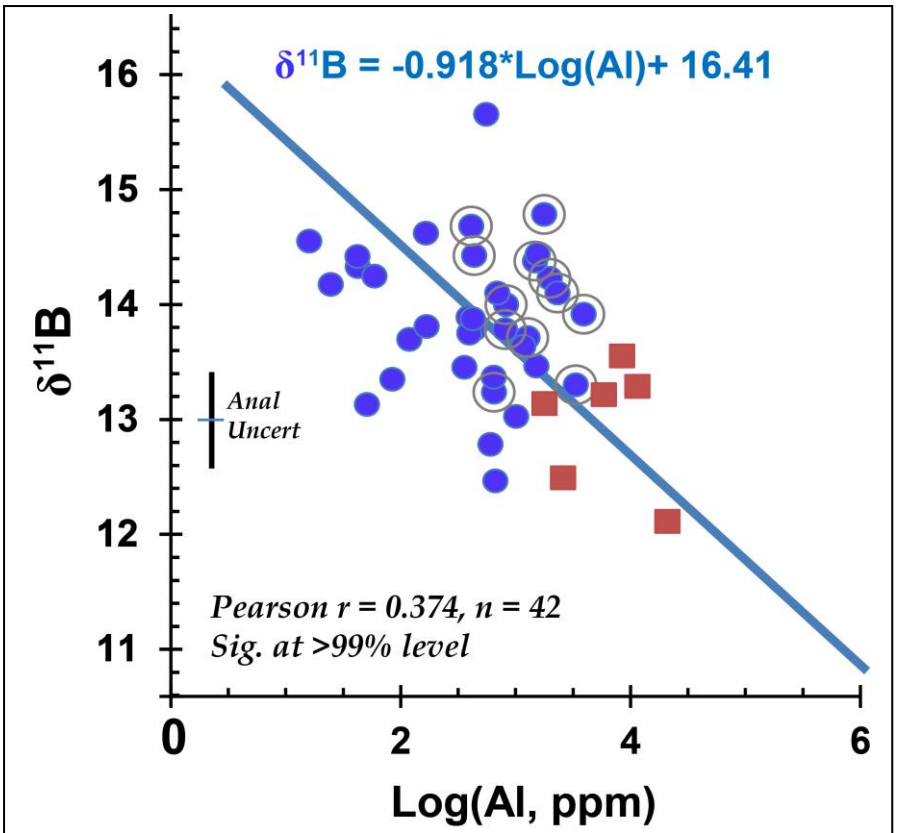

Fig. S6. Relation of Al to $\delta^{11}B$ in the data of M20. Red squares fall on the regession line in Fig S4. Analysis of two different brachiopods from each of 5 separate levels provides a proxy for analytical reproducibility of the sample analysis; the mean deviation of those 5 twin-analyses from the individual means is ± 0.39 ‰, with individual twins differing by up to 1.4 ‰

Completeness of the Section at Peniche.

The Peniche Section is the GSSP for the Toarcian. It contravenes rule 4, 7 and 8 of the set out by the ICS for choice of a GSSP (reproduced in blue italics below from https://stratigraphy.org/gssps/, accessed on 10/09 2020)

Global Boundary Stratotype Section and Points

Rules

A geologic section has to fulfil a set of criteria to be adapted as a GSSP by the ICS. The following list summarizes the criteria:

1. ***A GSSP has to define the lower boundary of a geologic Stage.***
2. ***The lower boundary has to be defined using a primary marker (usually first appearance datum of a fossil species).***
3. ***There should also be secondary markers (other fossils, chemical, geomagnetic reversal).***
4. ***The horizon in which the marker appears should have minerals that can be radiometrically dated.***
5. ***The marker has to have regional and global correlation in outcrops of the same age.***
6. ***The marker should be independent of facies.***
7. ***The outcrop has to have an adequate thickness.***
8. ***Sedimentation has to be continuous without any changes in facies***
9. ***The outcrop should be unaffected by tectonic and sedimentary movements, and metamorphism***
10. ***The outcrop has to be accessible to research and free to access. This includes that the outcrop has to be located where it can be visited quickly (international airport and good roads), has to be kept in good condition (ideally a national reserve), in accessible terrain, extensive enough to allow repeated sampling and open to researchers of all nationalities.***

The Pl-To boundary interval at Peniche is marked by a hardground and extreme condensation, and the Tenuicostatum Zone is an interval of varying sedimentation rate (McArthur *et al.* 2020a). These facts compromise the age model developed for the interval by Muller *et al.* (2020), which is based on a cyclostratigraphic analysis of Peniche which ignores such pertinent observations.

To emphasise this point, we reproduce the following from McArthur *et al.* (2020a), together with Fig. 4 or those authors.

At Peniche, values of 87Sr/86Sr increase by 0.000 012 over the first 3 metres of section (Fig. 3) and then remain at 0.707 085 over the next 2.5 m (to 5.5 m). Upsection from 5.5 m to 11.1 m, the rate of increase in 87Sr/86Sr increases as level increases. It follows that the sedimentation rate through the Tenuicostatum Chronozone was lowest in the basal 3 m of the section, highest between 3 and 5.5 m, where 87Sr/86Sr remains constant, and decreased upward from 5.5 m to the base of the Serpentinum Chronozone at 11.1 m. Of the increase in 87Sr/86Sr of 0.000 023 though this chronozone, half occurs in the basal 3 m of the section, so half of Tenuicostatum time is compressed

(non-linearly) into this basal 3 m of section. Most of the rest of Tenuicostatum time is non-linearly recorded in the sediments between 5.5 and 11.1 m. These observations of varying sedimentation rates will affect any cyclostratigraphic interpretation of the section (Suan et al. 2008b, Huang and Hesselbo 2014, cf. Ruebsam et al. 2014) because cyclostatigraphy assumes that sediments accumulate without breaks and at a constant rate.

That the sedimentation rate was slowest in the basal 3 m of the section is no surprise: Elmi (2007) noted that Bed 15 is a "condensed interval" and that characteristics of the 5 beds in Bed 15a–15e "indicate a low sedimentation rate" and also that these beds "are capped by a hard ground (top surface of level 15e in Mouterde 1955…)". Our Sr-isotope data show that this condensation extends into the overlying 3 m of sediment with condensation intensity decreasing upwards. Condensation is confirmed by the relative thicknesses of the Mirabile and Semicelatum II Subchronozones at Peniche compared to elsewhere (Fig. 4). ……Given the condensed nature of the boundary intervals at Peniche and Almonacid de la Cuba, the use of these localities as global (Rocha et al. 2016) and auxiliary (Comas-Rengifo et al. 2010) stratotype sections-an- points may need further evaluation. Whilst faunal successions may appear complete at Peniche, GSSPs should be chosen so that mineralogical and geochemical studies of the boundary can be undertaken with confidence in addition to faunal studies, a possibility impaired by condensation.

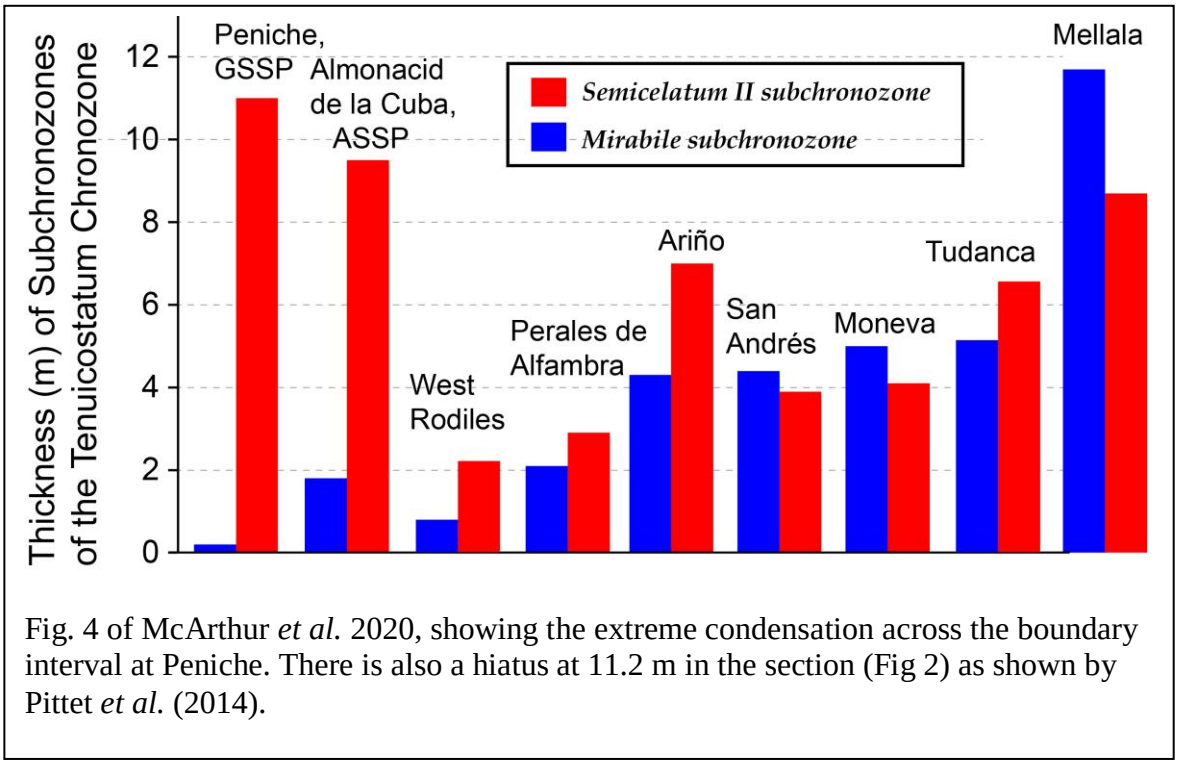

Fig. 4 of McArthur *et al.* 2020, showing the extreme condensation across the boundary interval at Peniche. There is also a hiatus at 11.2 m in the section (Fig 2) as shown by Pittet *et al.* (2014).

Additional References

Brand U. and Veizer J. 1980. Chemical diagenesis of a multicomponent carbonate system: 1. Trace elements. *J. Sediment. Petrol.* 50, 1219–1236.

Brand U. and Veizer J. 1981. Chemical diagenesis of a multicomponent carbonate system: 2. Stable isotopes. *J. Sediment. Petrol.* 51, 987–997.

McArthur, J.M., Howarth, R.J., Shields, G.A. and Zhou, Y. 2020b. Strontium isotope stratigraphy, Chapter 7, p*** – ***. In Gradstein F.M., Ogg J.G., Schmitz M.D. and Ogg G.M. A Geologic Time Scale, Elsevier B.V., Vol 1 of 2, *** pp, 2020.

Pittet, B., Suan, G., Lenoir, F., Duarte, L. V., Mattioli, L. V., 2014. Carbon isotope evidence for sedimentary discontinuities in the lower Toarcian of the Lusitanian Basin (Portugal): Sea level change at the onset of the Oceanic Anoxic Event. Sed. Geol. 303, 1–14.

Podlaha, O.G., Mutterlose, J., and Veizer, J. 1998. Preservation of $\delta^{18}O$ and $\delta^{13}C$ in belemnite rostra from the Jurassic/Early Cretaceous successions. *American Journal of Science*, **298**, 324–347.

Saelen, G. 1989. Diagenesis and construction of the belemnite rostrum. *Palaeontology*, **34(4)**, 765–798.